SELECTED STUDIES IN PHARMACEUTICS

By
Duoli Guo

_____

A Dissertation Submitted to the Faculty of the

DEPARTMENT OF PHARMACEUTICAL SCIENCES

In Partial Fulfillment of the Requirements

For the degree of

DOCTOR OF PHILOSOPHY

In the Graduate College

THE UNIVERSITY OF ARIZONA

2010

THE UNIVERSITY OF ARIZONA

GRADUATE COLLEGE

As members of the Dissertation Committee, we certify that we have read the dissertation prepared by Duoli Guo

entitled Selected Studies in Pharmaceutics

and recommend that it be accepted as fulfilling the dissertation requirement for the Degree of Doctor of Philosophy

Dr. Samuel H Yalkowsky	Date: May 12th 2009
Dr. Michael Mayersohn	Date: May 12th 2009
Dr. Paul Myrdal	Date: May 12th 2009

Final approval and acceptance of this dissertation is contingent upon the candidate's submission of the final copies of the dissertation to the Graduate College.

I hereby certify that I have read this dissertation prepared under my direction and recommend that it be accepted as fulfilling the dissertation requirement.

Dissertation Director: Dr Samuel H Yalkowsky Date May 12th 2009

STATEMENT BY AUTHOR

This dissertation has been submitted in partial fulfillment of requirements for an advanced degree at The University of Arizona and is deposited in the University Library to be made available to borrowers under rules of the Library.

Brief quotations from this thesis are allowable without special permission provided that accurate acknowledgment of source is made. Requests for permission for extended quotation from or reproduction of this manuscript in whole or in part may be granted by the head of the major department or the Dean of Graduate College when in his or her judgment the proposed use of the material is in the interests of scholarship. In all other instances, however, permission must be obtained from the author.

SIGNED: Duoli Guo

ACKNOWLEDGEMENTS

I would like to express my gratitude to my advisor, Dr. Samuel Yalkowsky, for his support, patience, and encouragement throughout my doctoral work. It is not often that one finds an advisor that always finds the time for the students. He has greatly assisted me with scientific writing and presentation. His technical and editorial advice was essential to the completion of this dissertation. He gave me many life wisdom as well as the insights on the academic research.

My thanks also go to the members of my major committee, Dr. Mayersohn, Dr. Myrdal, Dr. Loy and Dr. Ela for their time to serve on my committee.

I extend appreciation to my colleagues for their help and support during my graduate studies. They make my gradate studying a fun and enjoyable experience.

I have deepest gratitude towards my family. My parents have always been supportive. They taught me many good lessons. I will specially like to thank my sister and brother in law. Without their support, this would not have been possible. Their words of encouragement have always helped my self-confidence.

DEDICATION

TO MY PARENTS

TABLE OF CONTENTS

LIST OF FIGURES

LIST OF TABLES

ABSTRACT

Three different studies are included in this dissertation.

The first chapter is a preformulation study of the anticancer drug NSC-726796. A stability-indicating HPLC method to quantify the compound and its three main degradation products was developed. This method was used to investigate its degradation kinetics and mechanism. The reaction follows first-order kinetics and appears to be base-catalyzed with a maximum stability at pH 1. The degradation products were identified as 2-(2,4-difluorophenylcarbamoyl)-3,4,5,6-tetrafluorobenzoic acid (NSC-749820), 2,4-difluoroaniline and 3,4,5,6-tetrafluorophthalic acid. The mono acid was synthesized and its structure was confirmed by single crystal crystallography. That compound is found to be more soluble and more stable than the parent drug in aqueous media.

The purpose of the research reported in the second chapter is to investigate the pH-stability of an anticancer cytidine derivative and a cytidine deaminase inhibitor, individually and in combination. A stability indicating HPLC method for the quantification of 5-fluoro-2′-deoxycytidine (FdCyd, NSC-48006), tetrahydrouridine (THU, NSC-112907) and their degradants was developed using a ZIC®-HILIC column. The effect of THU and FdCyd on the *in vitro* degradation of each other was studied as a function of pH from 1.0 to 7.4. The degradation of FdCyd appears to be first-order and acid-catalyzed. THU equilibrates with at least one of its degradants. Results show that the combination of FdCyd and THU in solution does not affect the stability of either

compound. The stability and compatibility of FdCyd and THU in the solid state at 40 °C/ 75% relative humidity (RH) and at ambient temperature are also evaluated.

In chapter three, the effect of polarity on acid-base dissociation in ionic micellar systems is discussed. The dissociation constant of a compound (i.e., pK_a) can shift when it is incorporated in or on a micelle. The magnitude of the pK_a shift can be attributed to the effect of the surface potential of the micelle and the dielectric constant of the system. Currently, there is no reliable relationship to quantitate the dependence of ΔpK_a on the polarity of the drug. Experimental data for ΔpK_a of acids in cationic and anionic micelles were compiled from the literature. The increase in the pK_a of weak acids upon incorporation into sodium dodecyl sulphate micellar is shown to be proportional to their ClogP values.

CHAPTER 1: PREFORMULATION STUDY OF NSC-726796

1.1 Introduction:

The thalidomide analogue NSC-726796, also known as CPS49, is currently being investigated by the National Cancer institute (NCI) for its anticancer activity. It demonstrates direct cytotoxic effects against lymphocytic leukemia cells, as well as multiple myeloma, lung cancer, prostate cancer and endothelial cells [1-6]. The purpose of this study is to develop a stability-indicating high performance liquid chromatography method for the quantitation of NSC-726796 and to determine the effect of solution pH and polarity on its stability. The chemical structure of NSC-726796 is shown below. It is a substituted phthalimide with a melting point of 144 °C, molecular weight of 331, and a calculated Octanol/Water partition coefficient (ClogP) of 3.26. It is not ionizable in the 1 to14 pH range.

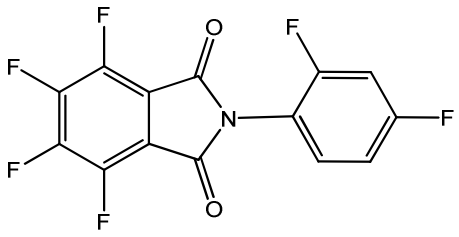

NSC-726796

1.2 Methods:

1.2.1 Chemicals and Reagents:

NSC-726796 was provided by the Pharmaceutical Resources Branch, National Cancer Institute (Bethesda, MD). Hydrochloric acid, phosphoric acid, sodium hydroxide, sodium phosphate, tetraflurophthalic anhydride and dichloromethane were purchased from Sigma-Aldrich (St. Louis, MO). Glacial acetic acid and citric acid monohydrate were purchased from Mallinckrodt (Paris, KY). Sodium chloride and acetonitrile were obtained from Fisher Chemicals (Fair Lawn, NJ). 2,4-difluoroaniline and 4-dimethylaminopyridine were purchased from Fluka. All agents were used without further purification. Water was purified using a Milli-Q system (18.2MΩ cm, Millipore, Billerica, MA).

1.2.2 Analytical Procedures:

1.2.2.1 High Performance Liquid Chromatography:

An Agilent 1100 HPLC (Agilent Technologies, Santa Clara, CA) system equipped with a quaternary pump, an automatic injector, a diode array wavelength detector, and ChemStation® software was used. A Discover HS F5 column (4.6mm×150mm) was used with an isocratic mobile phase composed of acetonitrile/ 0.1% TFA; 60/ 40. The flow rate was 0.5 ml/min, column temperature was 20 °C and the injection volume was 5 µl. The UV detection wavelength was set at 222 nm with 360 nm as the reference. When

necessary, samples were diluted in pure acetonitrile before being injected. Each peak area was computed automatically by the integrator.

1.2.2.2 Mass Spectrometry:

MS analyses of degradation products of NSC-726796 were performed by infusing the collected HPLC fractions into an ABI/SCIEX 4000 QTRAP hybrid triple-quadrupole linear ion trap mass spectrometer (Applied Biosystems, Foster City, CA) with electrospray ionization.

1.2.2.4 Differential Scanning Calorimetry:

The DSC thermograms of the solid samples were obtained using a Q1000 differential scanning calorimeter (TA Instruments, New Castle, DE) equipped with Universal Analysis 2000 software. Approximately 5mg of the drug was sealed in a hermetically crimped aluminum pan. The sample was heated with a linear ramp of 5 °C /min and purged with nitrogen at a flow rate of 40 mL/min. The melting temperature was noted as the point on the temperature scale corresponding to the maximum deviation from the baseline.

1.2.3 Experimental Procedures:

1.2.3.1 Reaction Kinetic Studies:

The formation of hydrolysis products of NSC-726796 was carried out in aqueous solutions at ambient temperature. A stock solution in acetonitrile was prepared at a

concentration of 50 mg/mL. The effect of pH on k_{obs} was determined using the buffer systems listed in Table 1. The ionic strength was maintained at 300mM using sodium chloride. Duplicates were prepared by quenching 10 µL of the stock solution in each buffer solution. The resulting solutions were immediately filtered through 0.45 µm filters and then injected for HPLC analysis.

1.2.3.2 Synthetic studies:

One of the hydrolysis products of NSC-726796, is the ring open acid, 2-(2,4-difluorophenylcarbamoyl)-3,4,5,6-tetrafluorobenzoic acid (DTA). Since it was not commercially available, it was synthesized by coupling tetraflurophthalic anhydride (1g, 4.54mmol) and 2,4-difluoroaniline (0.59g, 4.54mmol) using 4-dimethylaminopyridine (56mg, 0.454mmol) as the catalyst and dry dichloromethane (10ml) as the solvent. The mixture was stirred at ambient temperature for 72 hours. After the reaction was complete, the reaction mixture was partitioned between ethyl acetate and 2N HCl. The aqueous phase was then extracted twice more with ethyl acetate. The combined extracts were evaporated to a solid *in vacuo*. The solid was treated with diethyl ether at room temperature and the undissolved solids were discarded. The remaining solution was evaporated, and then triturated with cold diethyl ether to dissolve any remaining anhydride and filtered. The resulting white powder was analyzed by MS and NMR.

1.2.3.3 Reverse Reaction Kinetics at Low pH:

The reaction kinetics for conversion from ring open mono acid degradant to NSC-726796 was investigated in aqueous solutions at pH 1 and 2.5. Aliquots (10 µL) of a stock solution of the mono acid in acetonitrile were quenched with pH 1 and 2.5 buffers. Duplicates for each pH were immediately filtered. The resulting solutions were analyzed by HPLC at various time intervals.

Table 1: List of buffer solutions prepared for stability studies.

pH	Buffer	Buffer strength (mM)	Ionic strength(mM)
1	HCl	100	300
2.5	Citrate	100	300
4	Citrate	100	300
5.5	Citrate	100	300
7	Phosphate	100	300
8.5	Tris	100	300
10	Carbonate	100	300

1.3 RESULTS AND DISCUSSION:

1.3.1 HPLC Validation:

The retention time of NSC-726796 is approximately 12.2 min using the HPLC method described above. A representative chromatogram is shown in Figure 1a. The linear concentration range is 1-1000 µg/mL at 222 nm. The correlation coefficient (r^2) values are greater than 0.9999. The precision of intra-day and inter-day assay validation (indicated by standard deviation) is less than 5%.

1.3.2 Degradation of NSC-726796 in Alcohols:

The proposed reaction scheme of NSC-72796 with methanol is shown in Figure 2a. A similar reaction occurs when the drug is in contact with ethanol. Thus, these primary alcohols are not suitable for use as a mobile phase or a solubilization agent for the drug.

The methyl ester was isolated by dissolving NSC-726796 in methanol followed by slow evaporation of the solvent. The NMR results as well as the molecular weight determined by mass spectrometry are consistent with the structure provided in Figure 2a. When the methyl ester is dissolved in pure acetonitrile, there is some immediate conversion to the parent compound which becomes nearly complete after 4.5 hours as shown in Figure 1b and 1c.

1.3.3 Degradation of NSC-726796 in Aqueous Solutions:

NSC-726796 degrades reapidly upon contact with water. This is illustrated in Figure 5 by the representative HPLC chromatograms of the NSC-725796 in deionized (DI) water at 0, 15 and 45 min as well as at 21 days. The parent compound degrades to compound I, which elutes at 6.6 min and has a molecular weight of 349. In 15 minutes, most of the parent drug is lost. After 45 minutes, the loss is almost complete. Degradant I further degrades to II and III with retention time of 4.2 min and 6.2 min respectively. Degradant I was later confirmed to be 2-(2,4-difluorophenylcarbamoyl)-3,4,5,6-tetrafluorobenzoic acid by comparison to the synthesized compound (see below). Degradant II and III were identified as 3,4,5,6-tetrafluorophthalic acid and 2,4-difluoroaniline by mass spectrometry and by comparing their retention times and UV spectra with the reference compounds purchased from Sigma-Aldrich.

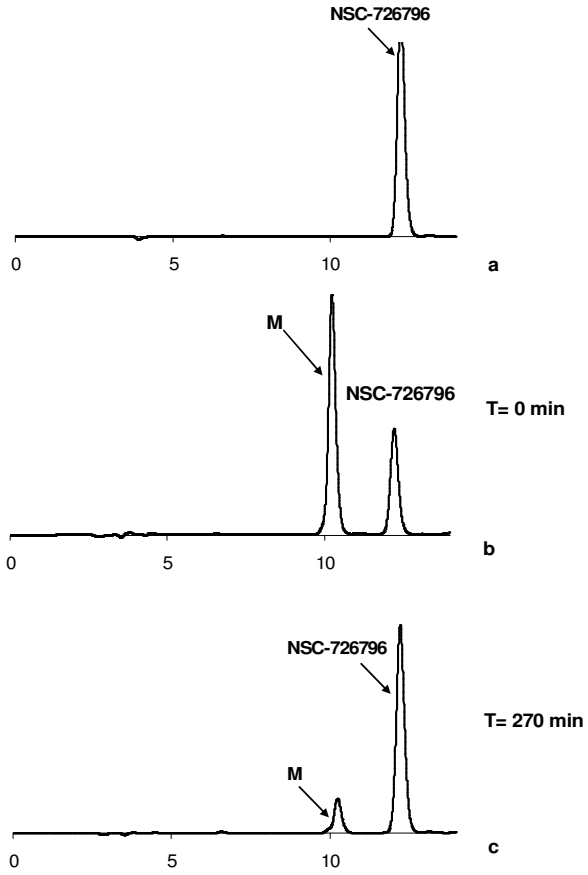

Figure 1: Chromatograms in acetonitrile (a) NSC-725796, (b) methyl ester 0 min, (c) methyl ester at 270 min.

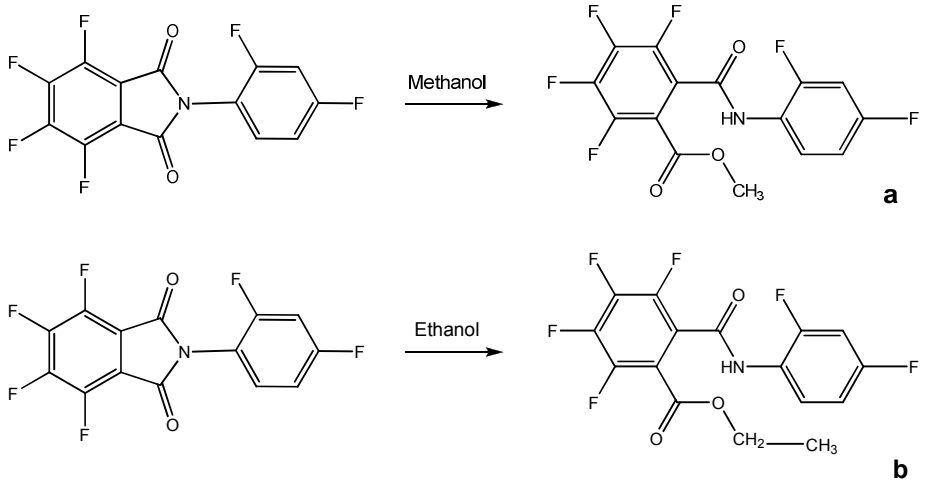

Figure 2: Degradation pathways of NSC-726796 in (a) methanol, (b) ethanol.

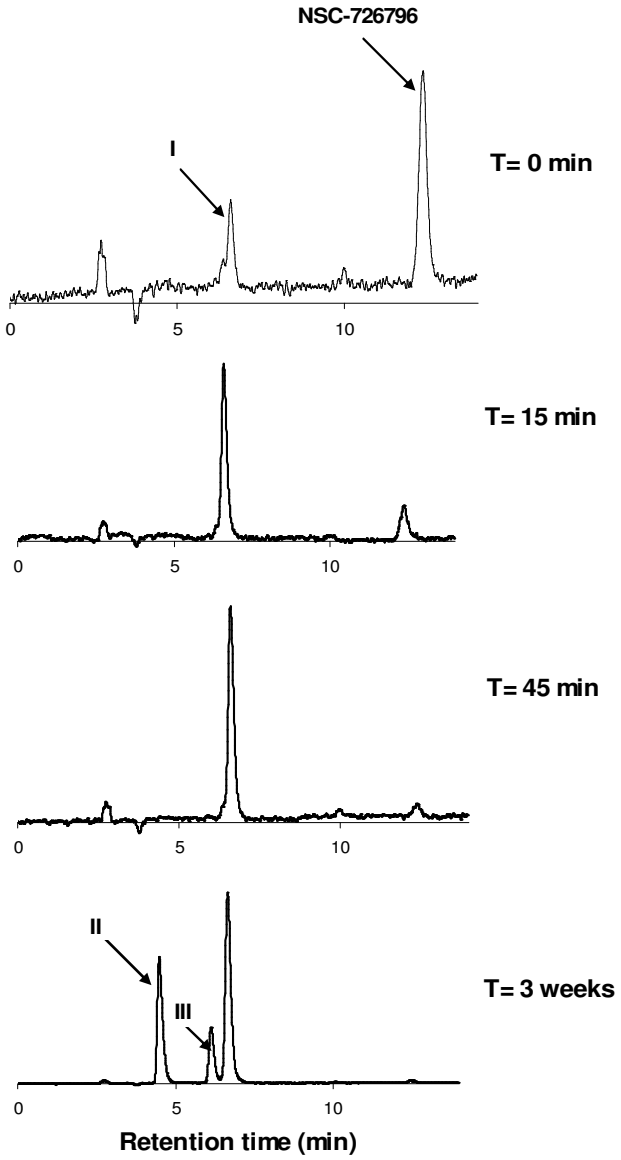

Figure 3: Chromatograms of NSC-725796 and degradants at different time.

1.3.4 Degradation Kinetics of NSC-726796 in Aqueous Solutions:

The stability of NSC-726796 at pHs 1, 2.5, 4, 5.5, 7, 8.5 and 10 was investigated for up to 6 hours. The percentage remaining in the solution is plotted in Figure 4 for each pH.

It is clear from Figure 4 that above pH 4 the degradation follows a first-order mechanism, where the slope corresponds to the $\left(k_{obs} / 2.303 \right)$ term in the following equation

$$\log[D] = \log[D_0] - \left(\frac{k_{obs}}{2.303} \right) t$$

$[D_0]$ and $[D]$ are the initial and time (t) dependent concentrations of drug, respectively, and k_{obs} is the observed degradation rate constant.

However, at pH 1 and 2.5, a slope change occurs after 200 min. Only the initial slope was used to calculate k_{obs}. Table 2 lists the degradation rate constant data at the investigated pH values. The reason for the slope change will be discussed later.

The k_{obs} values are plotted against pH in Figure 5. The degradation mechanism of the drug appears to be base catalyzed hydrolysis. It shows that the drug is more stable at pH 1 with about 50 % drug loss after 6 hours, while more than 90 % drug was lost at pH 5.5. The degradation rate above pH 8.5 was too fast to measure.

Table 2: Observed NSC-726796 degradation rate constants and half-lives in aqueous buffers.

pH	k_{obs} (min^{-1})	$T_{1/2}$ (min)
1	0.00276	334
2.5	0.00345	231
4	0.00415	167
5.5	0.00714	97
7	0.0263	26
8.5	Degrade too fast to quantitate	<5
10	Degrade too fast to quantitate	<1

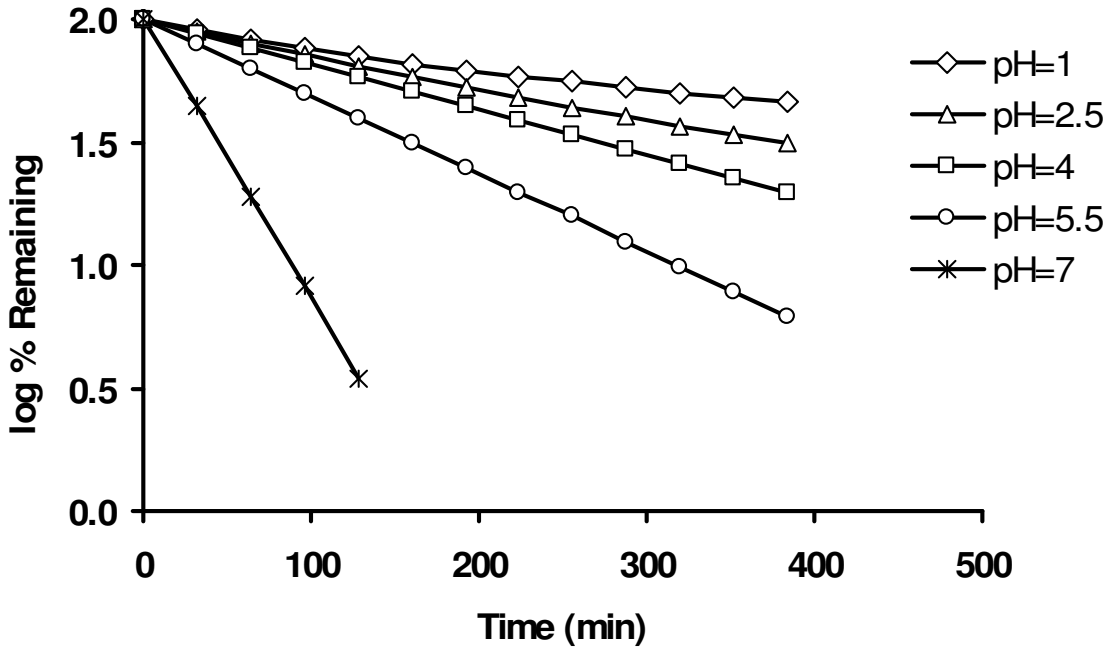

Figure 4: Percentage of NSC-726796 remaining (log scale) vs. time over 360 min.

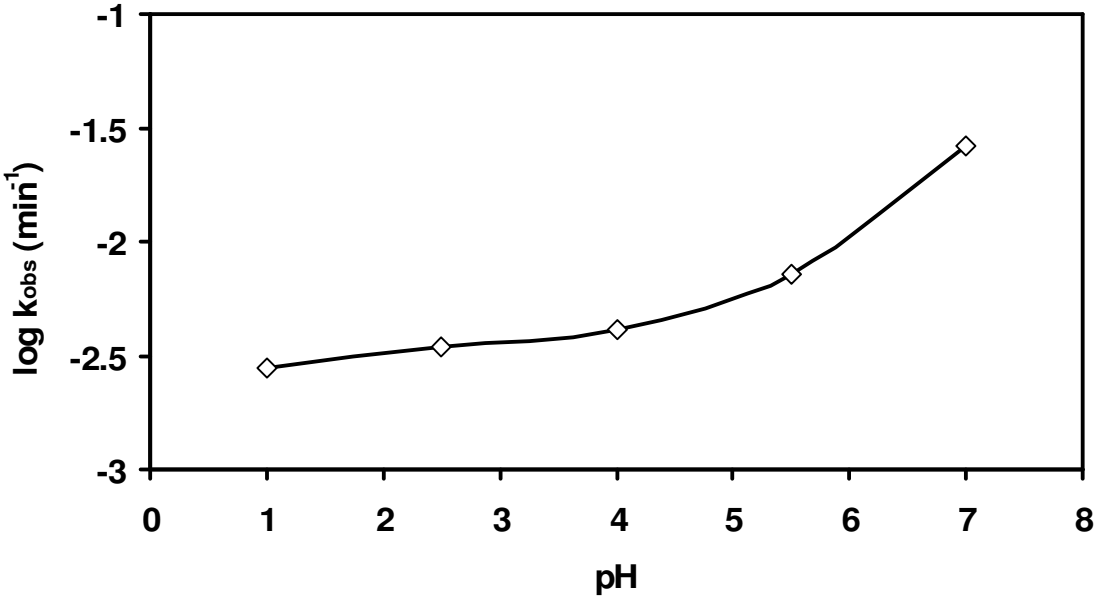

Figure 5: Degradation rate constant vs. pH of NSC-726796.

1.3.5 Synthesis of DTA:

A white powder was obtained using the synthetic scheme described in Figure 6. Mass spectrometry indicates the powder has a molecular weight of 349.18. The powder was assayed by HPLC and found to be greater than 97% pure. The major peak has the same retention time, spectrum and molecular weight as degradant I from NSC-726796 and the NMR results (not provided) are consistent with the proposed structure. The mono acid was assigned an internal identification number by National Cancer Institute as NSC-749820.

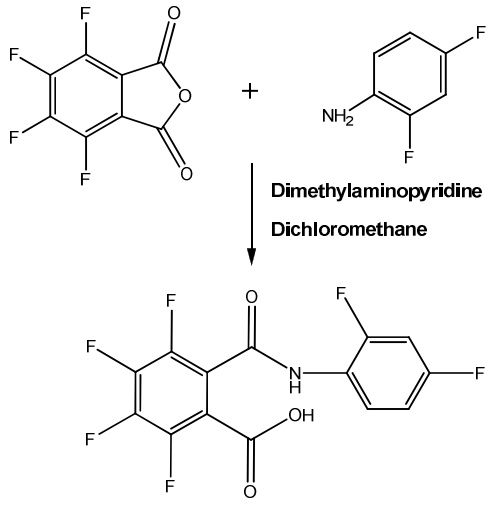

Figure 6: Synthetic scheme of DTA (NSC-749820).

1.3.6 Degradation Mechanism:

The degradation pathway of NSC-726796 is proposed in Figure 7. The phthalimide moiety is readily hydrolyzed to the mono acid NSC-749820. The mono acid degrades further by hydrolysis give 3,4,5,6-tetrafluorophthalic acid and 2,4-difluoroaniline later.

1.3.7 Reverse Reaction Kinetics at Low pH:

The slope change in the degradation of NSC-726796 at pHs 1 and 2.5 shown in Figure 5 is very likely due to the ring open degradant NSC-749820 converting back to the parent drug. To confirm this, the synthesized mono acid was dissolved in acetonitrile and then quenched with pH 1 buffer. These samples were filtered and analyzed by HPLC. The HPLC chromatogram in Figure 8a for a fresh solution at pH 1 shows only one peak for the ring open compound. Figure 8b shows that the ring closed form is present after one hour. Additional degradants, 3,4,5,6-tetrafluorophthalic acid and 2,4-difluoroaniline, appear after 4 hours as illustrated in Figure 8c. The amount of each compound was monitored at selected time intervals and plotted in Figure 9. The interconversion between the ring open and closed form was also observed at pH 2.5, but not at neutral and basic solutions. The partial conversion of mono acid compound to the parent drug at low pH can be ascribed to the acidic catalyzed esterification as the reversed reaction of hydrolysis illustrated in Figure 10. Mass balance of the reaction at pH 1 was confirmed.

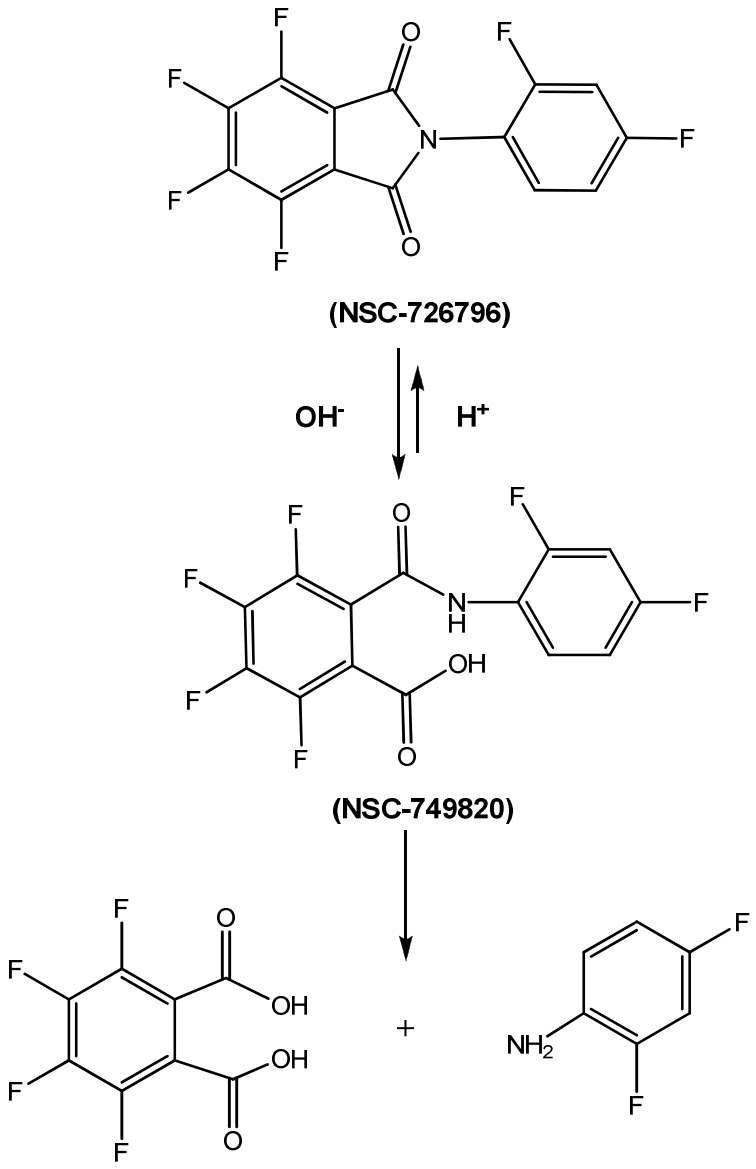

Figure 7: Degradation mechanism of NSC-72796.

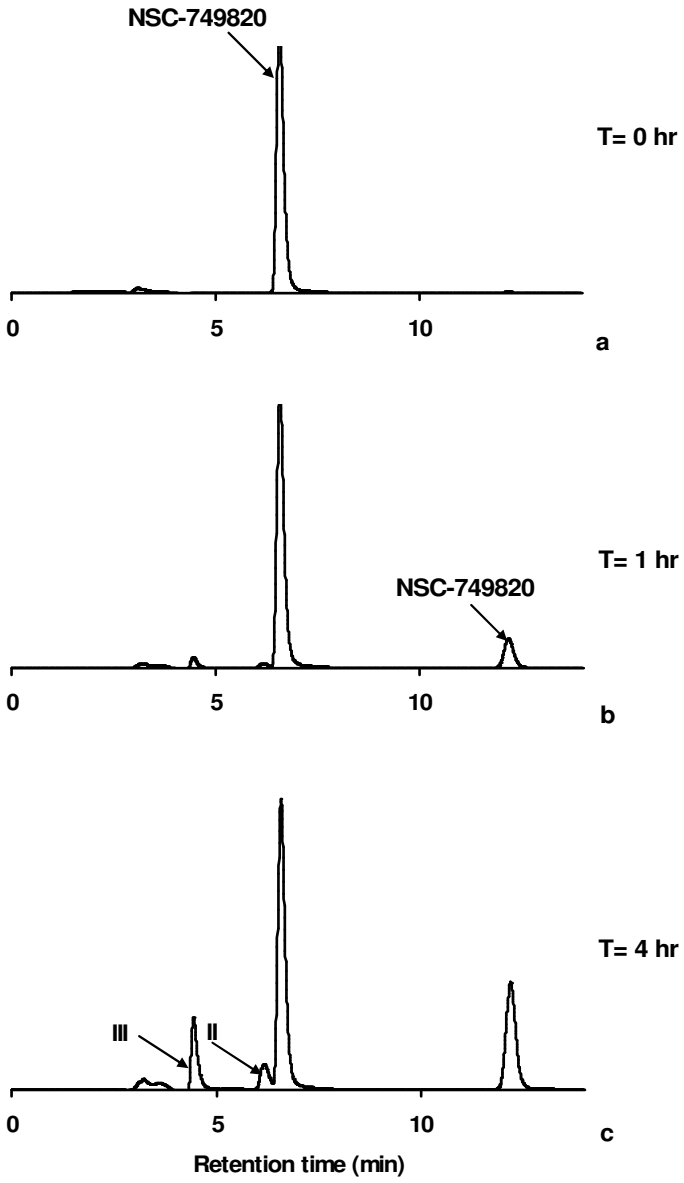

Figure 8: Chromatograms of NSC-749820 at pH 1.

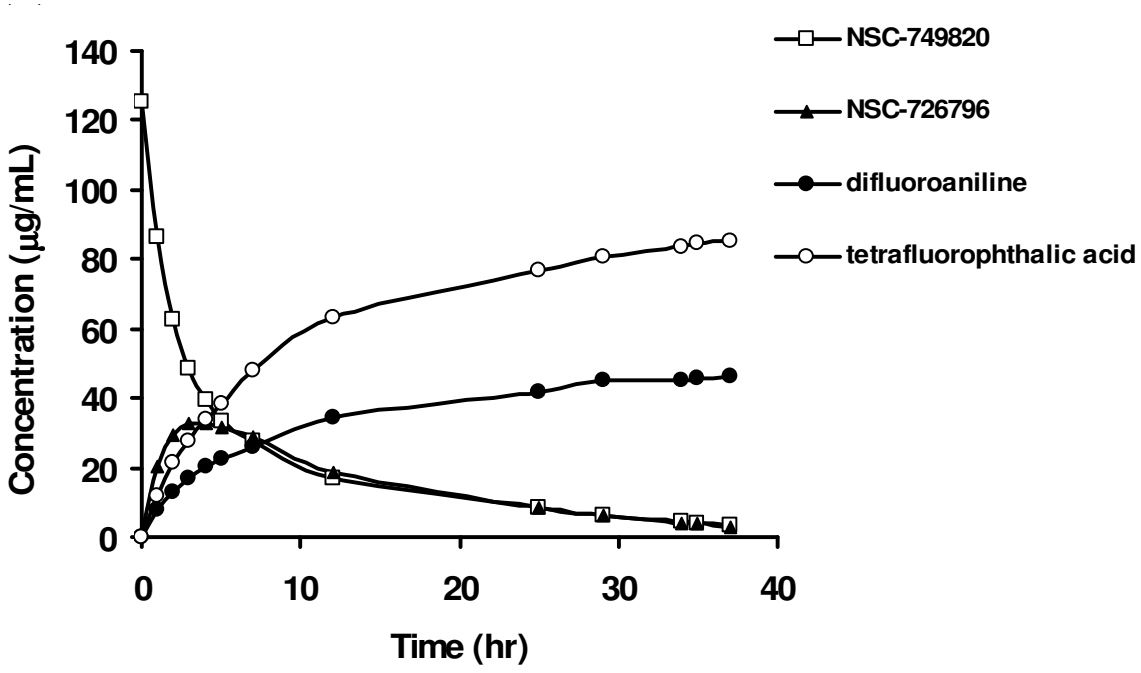

Figure 9: Conversion of NSC-749820 to phthalimide, 3,4,5,6-tetrafluorophthalic acid and 2,4-difluoroaniline at pH=1.

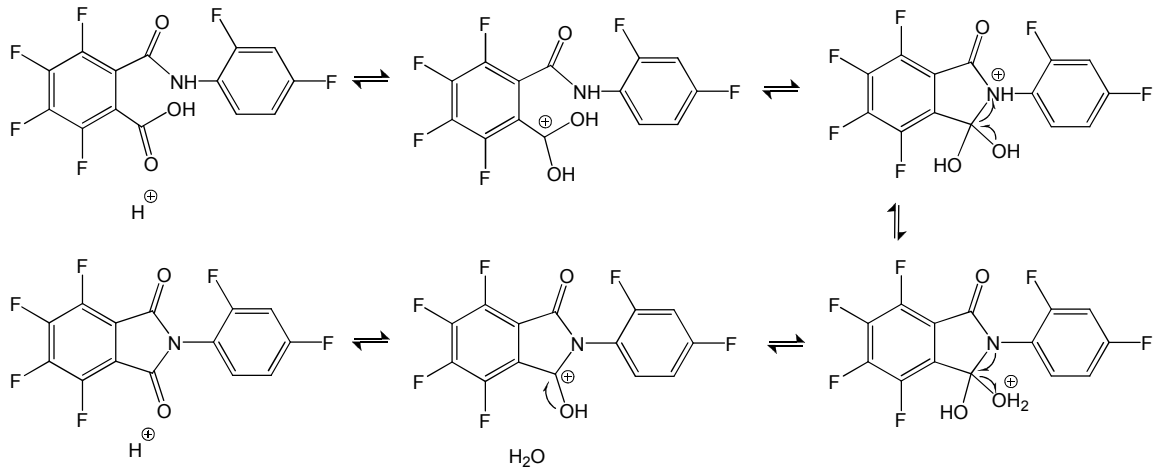

Figure 10: Hydrolysis of phthalimide and esterification of the mono acid.

1.3.8 DSC Results:

DSC studies of both compounds shown in Figure 11 indicate that NSC-726796 and the degradant have a melting point of 144 °C and 169 °C, respectively. The higher melting point of the ring open compound is due to its ability to hydrogen bond, even though is has less symmetry than the parent phthalimide.

1.3.9 Rationale:

Due to the fact that NSC-726796 degrades instantaneously to the ring open mono acid compound upon contact with water, the latter may be responsible for the antitumor activity of the former. The ring open degradant is more polar (ClogP=1.60) than that of the parent compound (ClogP=3.26). Using the general solubility equation [7] and the melting points shown above, the intrinsic solubility of ring open degradant is about 100 times higher than the parent drug. Furthermore, while NSC-726796 is not ionizable between pH 1-14, the mono acid degradant has an acidic pK_a of 1.79 and it will be largely ionized and more soluble at blood pH. If NSC-749820 is active, it might be a better form to formulate. This compound is currently under evaluation for anticaner activity by the National Cancer Institute.

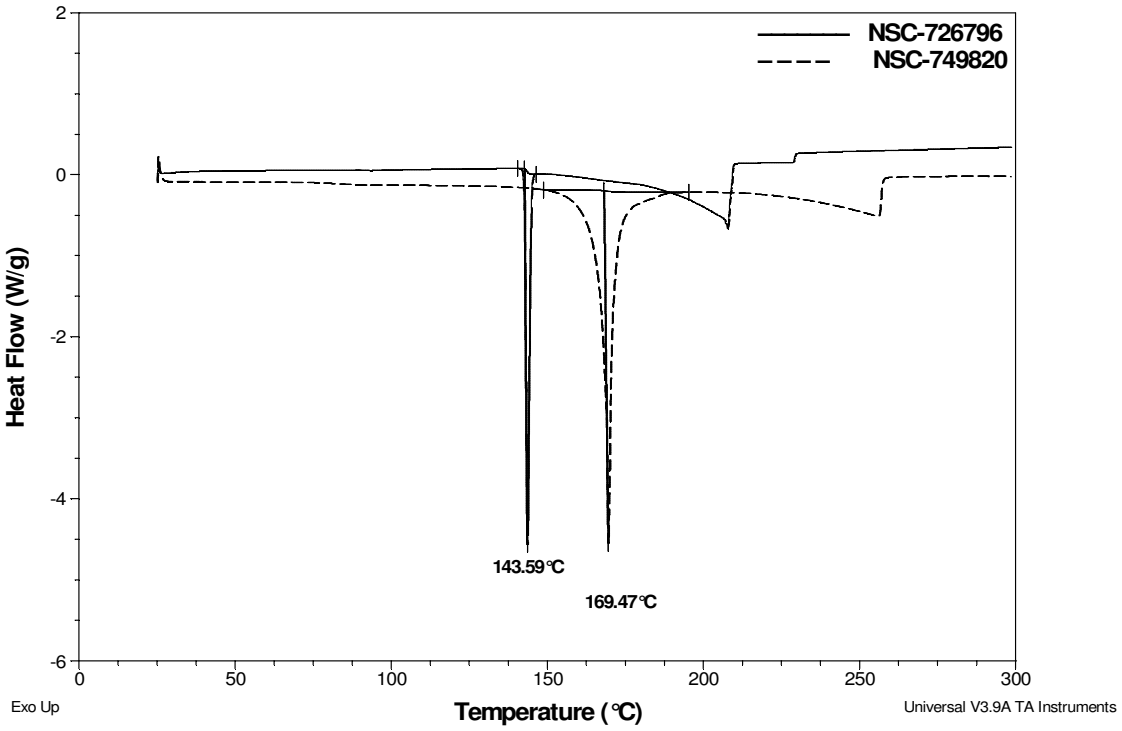

Figure 11: DSC thermograms of NSC-726796 and NSC-749820.

1.3.10 Structure Identification of DTA:

Compound 2-(2,4-difluorophenylcarbamoyl)-3,4,5,6-tetrafluorobenzoic acid (DTA) was provided as small needle and prism-like crystals. Both crystal morphologies have the same unit cell parameters and data were collected on a prism crystal. Although the crystal was reasonably large the diffraction was phenomenally weak. With 60 second exposures using copper radiation data could only be observed up to a resolution of 1Å; the dataset was truncated at this resolution. The diffraction pattern is a non-merohedral twin with a refined twin fraction ratio of 0.46. A room temperature redetermination of the unit cell, using a fresh crystal, showed that twinning was still present and does not result from flash-cooling to 100 K. Crystal data and structure refinement for DTA are listed in Table 3.

Structure shy103 features two crystallographically-independent molecules in the asymmetric unit. Structural discussion is limited to molecule A. The molecular structures of molecule A and B are shown in Figure 12. The plane of the more highly-substituted aryl ring is rotated by 69.41(45)° [69.64(39)°] from the amide group, and the carboxylic acid group is rotated by 58.70(23)° [61.10(25)°] from the aryl ring. The plane of the second aryl ring is rotated by 70.25(43)° [66.54(42)°] from the amide group. As can be see from Table 4 the direction of rotation is different for each molecule, most easily appreciated by considering the torsion angle N(1)–C(1)–C(2)–C(3) –49.0(8)° [48.5(10)°] (similar magnitude, opposite direction).

As shown in Figures 13 the compound packs as a double tape structure with each crystallographically-unique molecule hydrogen-bonded to its symmetry equivalents *via* O–H···O and N–H···O hydrogen bonding interactions (Table 5). Each tape runs parallel to the *a* axis.

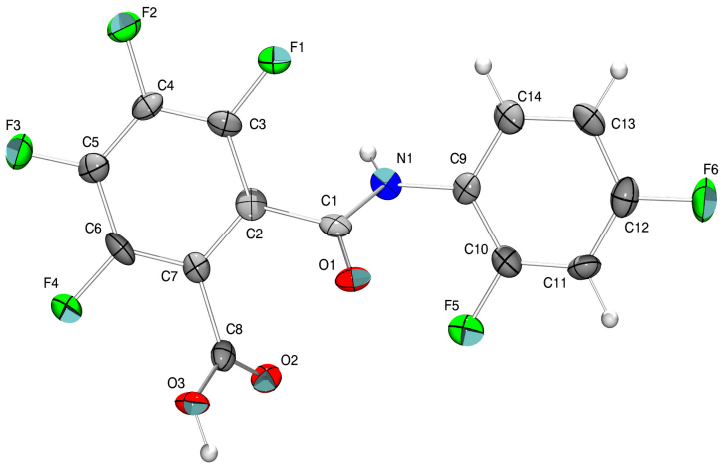

(a)

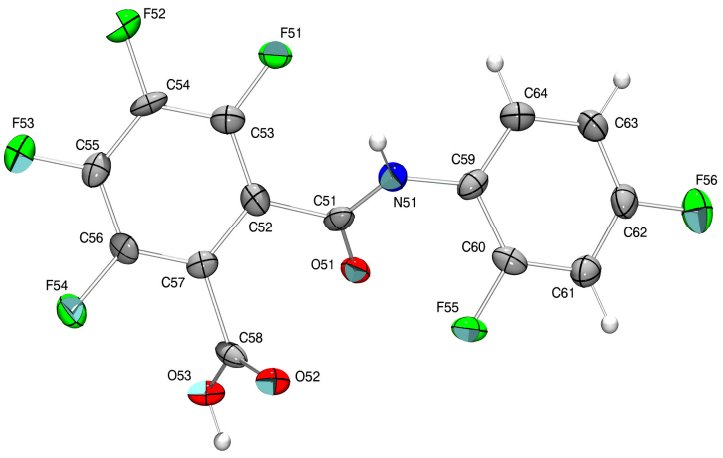

(b)

Figure 12: The molecular structure of A and B, with anisotropic displacement ellipsoids at the 50% probability level.

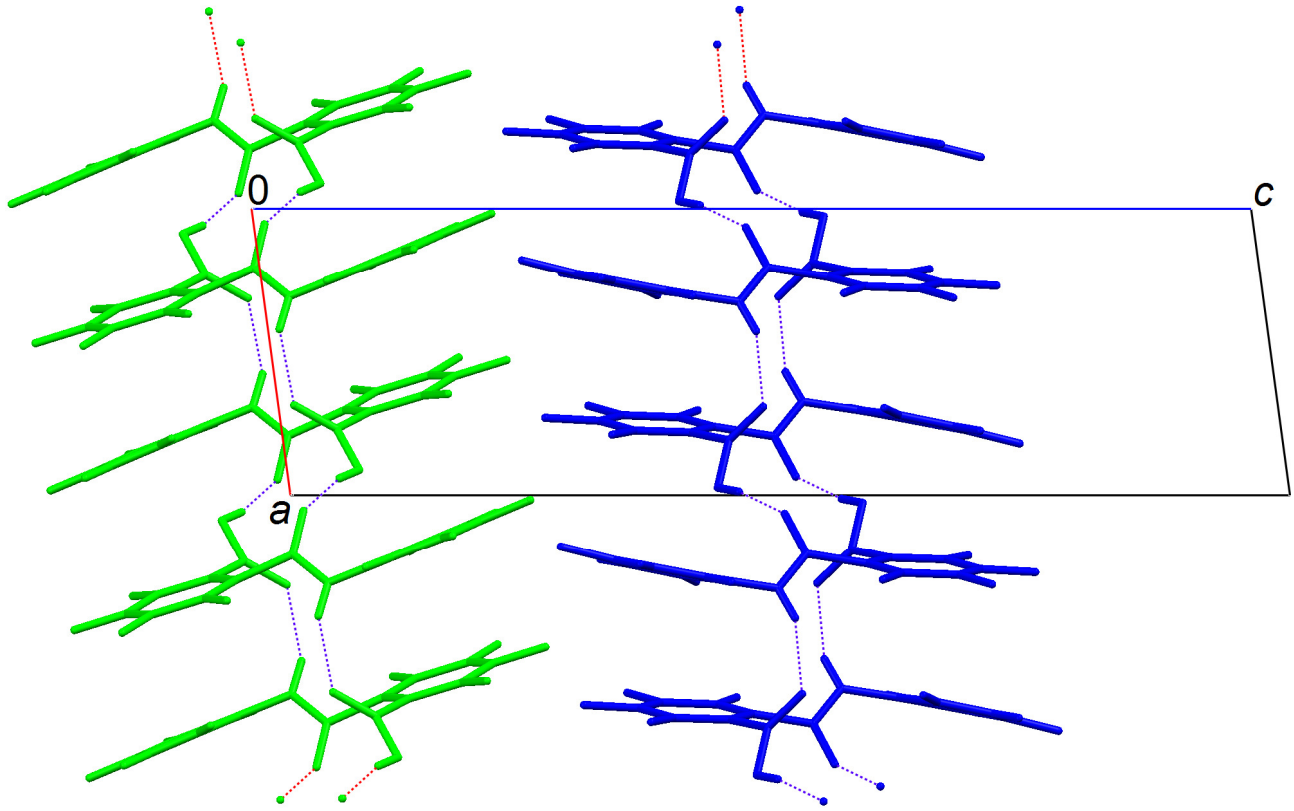

Figure 13: A b-axis projection of the crystal packing in shy103.

Table 3: Crystal data and structure refinement for shy103.

Identification code	shy103	
Chemical formula (moiety)	$C_{14}H_5F_6NO_3$	
Chemical formula (total)	$C_{14}H_5F_6NO_3$	
Formula weight	349.19	
Temperature	100(2) K	
Radiation, wavelength	CuKα, 1.54178 Å	
Crystal system, space group	Triclinic, $P\bar{1}$	
Unit cell parameters	a = 7.5293(4) Å	α = 89.809(5)°
	b = 7.6795(5) Å	β = 82.747(4)°
	c = 24.1969(15) Å	γ = 68.712(4)°
Cell volume	1291.83(13) $Å^3$	
Z	4	
Calculated density	1.795 g/cm^3	
Absorption coefficient μ	1.652 mm^{-1}	
F(000)	696	
Crystal colour and size	colourless, 0.27 × 0.19 × 0.09 mm^3	
Reflections for cell refinement	617 (θ range 3.7 to 56.9°)	
Data collection method	Bruker Kappa APEXII DUO CCD diffractometer ϕ and ω scans	
θ range for data collection	1.8 to 58.5°	
Index ranges	h −8 to 8, k −8 to 8, l 0 to 26	
Completeness to θ = 58.5°	89.9 %	
Reflections collected	7781	
Independent reflections	3296 (R_{int} = 0.0740)	
Reflections with $F^2>2\sigma$	2467	
Absorption correction	numerical	
Min. and max. transmission	0.6640 and 0.8683	
Structure solution	direct methods	
Refinement method	Full-matrix least-squares on F^2	
Weighting parameters a, b	0.1222, 0.0000	
Data / restraints / parameters	3296 / 0 / 434	
Final R indices [$F^2>2\sigma$]	R1 = 0.0665, wR2 = 0.1720	
R indices (all data)	R1 = 0.0847, wR2 = 0.1820	
Goodness-of-fit on F^2	0.993	
Largest and mean shift/su	0.000 and 0.000	
Largest diff. peak and hole	0.40 and −0.43 e $Å^{-3}$	

Table 4: Bond lengths [Å] and angles [°] for shy103.

F(1)–C(3)	1.342(8)	F(2)–C(4)	1.342(8)
F(3)–C(5)	1.326(8)	F(4)–C(6)	1.353(8)
F(5)–C(10)	1.364(8)	F(6)–C(12)	1.365(9)
O(1)–C(1)	1.230(9)	O(2)–C(8)	1.214(8)
O(3)–H(3)	0.840	O(3)–C(8)	1.309(8)
N(1)–H(1)	0.880	N(1)–C(1)	1.349(9)
N(1)–C(9)	1.416(9)	C(1)–C(2)	1.517(10)
C(2)–C(3)	1.388(10)	C(2)–C(7)	1.408(10)
C(3)–C(4)	1.369(10)	C(4)–C(5)	1.371(11)
C(5)–C(6)	1.400(11)	C(6)–C(7)	1.359(11)
C(7)–C(8)	1.506(10)	C(9)–C(10)	1.396(11)
C(9)–C(14)	1.391(10)	C(10)–C(11)	1.351(10)
C(11)–H(11)	0.950	C(11)–C(12)	1.357(11)
C(12)–C(13)	1.399(11)	C(13)–H(13)	0.950
C(13)–C(14)	1.378(11)	C(14)–H(14)	0.950
F(51)–C(53)	1.332(8)	F(52)–C(54)	1.336(8)
F(53)–C(55)	1.337(9)	F(54)–C(56)	1.348(8)
F(55)–C(60)	1.361(8)	F(56)–C(62)	1.367(9)
O(51)–C(51)	1.240(8)	O(52)–C(58)	1.195(9)
O(53)–H(53)	0.840	O(53)–C(58)	1.321(9)
N(51)–H(51)	0.880	N(51)–C(51)	1.341(10)
N(51)–C(59)	1.405(10)	C(51)–C(52)	1.504(10)
C(52)–C(53)	1.375(11)	C(52)–C(57)	1.401(10)
C(53)–C(54)	1.384(11)	C(54)–C(55)	1.393(11)
C(55)–C(56)	1.366(11)	C(56)–C(57)	1.371(11)
C(57)–C(58)	1.532(10)	C(59)–C(60)	1.390(10)
C(59)–C(64)	1.391(11)	C(60)–C(61)	1.378(11)
C(61)–H(61)	0.950	C(61)–C(62)	1.383(11)
C(62)–C(63)	1.348(11)	C(63)–H(63)	0.950
C(63)–C(64)	1.366(11)	C(64)–H(64)	0.950

H(3)–O(3)–C(8)	109.5	H(1)–N(1)–C(1)	118.5
H(1)–N(1)–C(9)	118.5	C(1)–N(1)–C(9)	123.0(6)
O(1)–C(1)–N(1)	125.2(7)	O(1)–C(1)–C(2)	119.4(6)
N(1)–C(1)–C(2)	115.4(6)	C(1)–C(2)–C(3)	122.6(6)
C(1)–C(2)–C(7)	118.8(6)	C(3)–C(2)–C(7)	118.1(7)
F(1)–C(3)–C(2)	120.4(7)	F(1)–C(3)–C(4)	118.0(6)
C(2)–C(3)–C(4)	121.6(7)	F(2)–C(4)–C(3)	119.8(6)
F(2)–C(4)–C(5)	119.4(6)	C(3)–C(4)–C(5)	120.8(7)
F(3)–C(5)–C(4)	121.4(7)	F(3)–C(5)–C(6)	120.7(7)
C(4)–C(5)–C(6)	117.9(7)	F(4)–C(6)–C(5)	116.7(7)
F(4)–C(6)–C(7)	120.9(7)	C(5)–C(6)–C(7)	122.3(7)
C(2)–C(7)–C(6)	119.4(7)	C(2)–C(7)–C(8)	119.5(6)
C(6)–C(7)–C(8)	121.0(6)	O(2)–C(8)–O(3)	125.7(7)

O(2)–C(8)–C(7)	122.0(6)	O(3)–C(8)–C(7)	112.3(6)
N(1)–C(9)–C(10)	122.7(6)	N(1)–C(9)–C(14)	119.7(6)
C(10)–C(9)–C(14)	117.5(7)	F(5)–C(10)–C(9)	118.0(6)
F(5)–C(10)–C(11)	118.8(6)	C(9)–C(10)–C(11)	123.2(7)
C(10)–C(11)–H(11)	121.2	C(10)–C(11)–C(12)	117.6(7)
H(11)–C(11)–C(12)	121.2	F(6)–C(12)–C(11)	119.5(7)
F(6)–C(12)–C(13)	117.6(7)	C(11)–C(12)–C(13)	122.9(7)
C(12)–C(13)–H(13)	121.1	C(12)–C(13)–C(14)	117.8(7)
H(13)–C(13)–C(14)	121.1	C(9)–C(14)–C(13)	120.9(7)
C(9)–C(14)–H(14)	119.6	C(13)–C(14)–H(14)	119.6
H(53)–O(53)–C(58)	109.5	H(51)–N(51)–C(51)	118.6
H(51)–N(51)–C(59)	118.6	C(51)–N(51)–C(59)	122.7(6)
O(51)–C(51)–N(51)	122.9(6)	O(51)–C(51)–C(52)	118.8(7)
N(51)–C(51)–C(52)	118.2(6)	C(51)–C(52)–C(53)	122.1(7)
C(51)–C(52)–C(57)	118.6(6)	C(53)–C(52)–C(57)	119.0(7)
F(51)–C(53)–C(52)	121.6(6)	F(51)–C(53)–C(54)	117.7(7)
C(52)–C(53)–C(54)	120.7(7)	F(52)–C(54)–C(53)	120.1(7)
F(52)–C(54)–C(55)	119.9(7)	C(53)–C(54)–C(55)	119.9(7)
F(53)–C(55)–C(54)	119.4(7)	F(53)–C(55)–C(56)	121.4(7)
C(54)–C(55)–C(56)	119.1(7)	F(54)–C(56)–C(55)	117.6(6)
F(54)–C(56)–C(57)	120.8(7)	C(55)–C(56)–C(57)	121.5(7)
C(52)–C(57)–C(56)	119.8(7)	C(52)–C(57)–C(58)	120.1(6)
C(56)–C(57)–C(58)	120.1(7)	O(52)–C(58)–O(53)	127.9(7)
O(52)–C(58)–C(57)	122.0(7)	O(53)–C(58)–C(57)	110.1(7)
N(51)–C(59)–C(60)	120.9(7)	N(51)–C(59)–C(64)	121.8(7)
C(60)–C(59)–C(64)	117.2(7)	F(55)–C(60)–C(59)	119.2(6)
F(55)–C(60)–C(61)	117.9(7)	C(59)–C(60)–C(61)	122.9(7)
C(60)–C(61)–H(61)	122.0	C(60)–C(61)–C(62)	116.0(7)
H(61)–C(61)–C(62)	122.0	F(56)–C(62)–C(61)	117.0(7)
F(56)–C(62)–C(63)	119.6(7)	C(61)–C(62)–C(63)	123.4(7)
C(62)–C(63)–H(63)	120.4	C(62)–C(63)–C(64)	119.3(7)
H(63)–C(63)–C(64)	120.4	C(59)–C(64)–C(63)	121.0(7)
C(59)–C(64)–H(64)	119.5	C(63)–C(64)–H(64)	119.5

Table 5: Hydrogen coordinates and isotropic displacement parameters (Å^2) for shy103.

	x	y	z	U
H(3)	0.9411	–0.1078	0.0513	0.034
H(1)	0.5782	0.6737	–0.0115	0.025
H(11)	0.9396	0.4074	–0.2032	0.035
H(13)	0.8582	0.9414	–0.1566	0.035
H(14)	0.7487	0.8899	–0.0655	0.034
H(53)	0.9875	–0.6255	0.4491	0.034
H(51)	0.5713	0.1778	0.5119	0.030
H(61)	0.7755	–0.0707	0.6986	0.037
H(63)	0.7575	0.4470	0.6595	0.036
H(64)	0.6955	0.4007	0.5706	0.036

Table 6: Hydrogen bonds [Å] and angle for shy103 [°].

D–H···A	d(D–H)	d(H···A)	d(D···A)	<(DHA)
O(3)–H(3) ···O(1A)	0.84	1.84	2.666(6)	168
N(1)–H(1) ···O(2B)	0.88	2.09	2.902(7)	153
O(53)–H(53) ···O(51C)	0.84	1.84	2.675(6)	170
N(51)–H(51) ···O(52D)	0.88	2.07	2.902(8)	157

Symmetry operations for equivalent atoms
A −x+2,−y,−z B −x+1,−y+1,−z C −x+2,−y−1,−z+1
D −x+1,−y,−z+1

1.4 CONCLUSION:

The hydrolytic degradation kinetics and mechanism of NSC-726796 were investigated at various pH values at ambient temperature. From the log k_{obs}-pH profile, it is concluded that the hydrolysis is mainly base-catalyzed. The ring open degradant was synthesized and identified as 2-(2,4-difluorophenylcarbamoyl)-3,4,5,6-tetrafluorobenzoic acid which is also know as NSC-749820. This mono acid can be converted back to NSC-72796 in acidic conditions, but eventually degrades to 3,4,5,6-tetrafluorophthalic acid and 2,4-difluoroaniline. NSC-74980 is currently under investigation for its anticancer activity.

CHAPTER 2: STABILITY STUDIES OF FdCyd AND THU IN COMBINATION

2.1 Introduction:

The nucleoside analogue 5-fluoro-2′-deoxycytidine (FdCyd, NSC 48006) is being evaluated clinically as a DNA methyltransferase inhibitor. Unfortunately, FdCyd undergoes rapid metabolism in vivo by cytidine deaminase [8]. Co-administration of FdCyd with tetrahydrouridine (THU), a cytidine deaminase inhibitor, prevents the rapid metabolism of FdCyd to its pharmacologically active metabolites and thus results in less side-effects and more efficient hypomethylation [9-11]. The purpose of this study is to investigate the pH-stability and solid state stability of the compounds individually and in combination. The chemical structures of FdCyd and THU are shown as below.

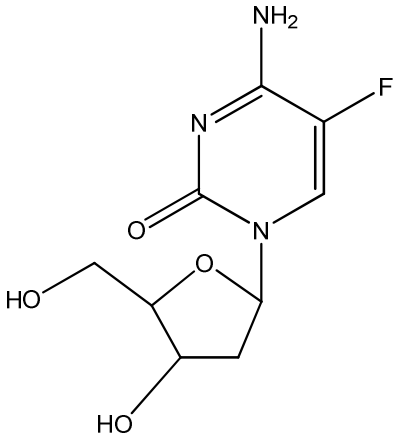

FdCyd

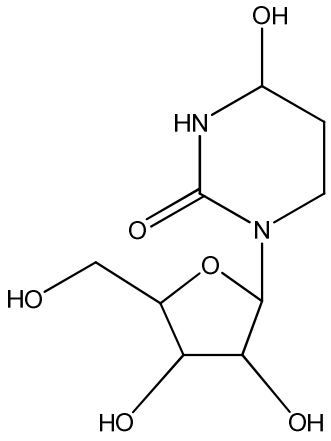

THU

2.2 Experimental:

2.2.1 Materials:

The FdCyd and THU were provided by the Pharmaceutical Resources Branch, National Cancer Institute (Bethesda, MD) and were used as received. Ammonium acetate, hydrochloric acid, phosphoric acid, sodium hydroxide, sodium phosphate and 5-fluorocytosine were purchased from Sigma-Aldrich (St. Louis, MO). Glacial acetic acid and citric acid monohydrate were purchased from Mallinckrodt (Paris, KY). Sodium chloride and acetonitrile were obtained from Fisher Chemicals (Fair Lawn, NJ). All agents were of analytical grade and used without further purification. Water was purified using a Milli-Q system (18.2MΩ cm, Millipore, Billerica, MA).

2.2.2 Buffer Preparation:

The buffer systems used for pH stability profile studies are listed in Table 1. The ionic strength was maintained at 300mM by adding sodium chloride.

Table 7: List of buffer solutions prepared for stability studies.

pH	Buffer	Buffer strength (mM)	Ionic strength(mM)
1	HCl	100	300
2	Phosphate	100	300
3	Citrate	100	300
4	Citrate	100	300
5	Citrate	100	300
7.4	Phosphate	100	300

2.2.3 High Performance Liquid Chromatography Optimization:

Reverse phase C18 and C8 columns provided poor retention for FdCyd and THU, which are polar compounds. A HILIC column was then chosen for this study since it is especially suitable for hydrophilic analytes. The mobile phase contained a high concentration of acetonitrile to promote interactions between the analytes and the stationary phase.

An Agilent 1100 HPLC (Agilent Technologies, Santa Clara, CA) system equipped with a quaternary pump, an automatic injector, a diode array detector, and ChemStation® software was used. A ZIC®-HILIC column (5 µm, 4.6 mm×150 mm) from Sequant AB (Umeå, Sweden) was used with a mobile phase composed of 85% acetonitrile for this study. The aqueous phase contained 25 mM acetic acid and 2.5 mM ammonium acetate. The flow rate was 0.5 ml/min, the column temperature was 20 °C and the injection volume was 10-40 µl. The UV detection wavelength was set at 210 nm with 360 nm as the reference. The HPLC assay developed in this study can detect FdCyd, THU and their major degradants.

2.2.4 Standard Solution:

A 15% deionized water in acetonitrile solution was used to prepare the standard solutions of FdCyd and THU. The solution polarity was consistent with the HPLC mobile phase. All standard solutions were prepared and measured in duplicate. The intra-day and inter-day precision of injection was evaluated.

2.2.5 Differential Scanning Calorimetry (DSC):

The DSC thermalgrams of the solid samples were obtained using a Q1000 differential scanning calorimeter (TA Instruments, New Castle, DE) equipped with TA Universal Analysis 2000 software. Samples with approximately 5 mg were sealed in hermetically crimped pans. DSC samples were heated at 5°C/min under nitrogen purge at a flow rate of 40 mL/min. The peak temperature was noted as the point corresponding to the onset of deviation from the baseline.

2.2.6 Thermogravimetric Analysis (TGA):

The TGA curves were obtained using a Q1000 thermogravimetric analyzer (TA Instruments, New Castle, DE) linked to TA Universal Analysis 2000 software. All TGA runs were performed on samples in open aluminum pans with a nitrogen purge at 60 mL /min. Nonisothermal TGA was performed on 5 mg samples at a heating rate of 5 °C/min.

2.2.7 Powder X-ray Diffractometry (PXRD):

The powder X-ray diffraction patterns of samples were determined at ambient temperature on a PANalytical MPD X'Pert Pro diffractometer with Cu Kalpha radiation, using a circular rotating sample holder, a scan range of 4-90 degrees 2theta, a scan step size of 0.004187 and a scan speed of 10.16 seconds per step.

2.2.8 Sample Preparation for pH Stability Studies:

Duplicate stock solutions containing 1 mg/mL of FdCyd and/or 5 mg/mL of THU were prepared using the buffer systems mentioned above. The solutions were stored in clear glass vials at 37 °C. The data were collected at different intervals over about 400 hours. The pH values of samples were checked and adjusted to within ± 0.2 units using concentrated HCl or NaOH.

2.2.9 Sample Preparation for Solid State Stability and Compatibility:

Ambient fluorescent light was used to study the effect of light on solid FdCyd, THU and the physical mixtures (1:5) with and without grinding. Ground samples were prepared by hand grinding using an agate mortar with a pestle. Control samples were kept in amber vials. For the thermal stability, samples were incubated at 40 °C/ 75% RH (which was maintained by a saturated solution of NaCl) for 1 month. The moisture absorption was monitored by following weight changes of samples that were loosely dispersed on a DSC aluminum pan to guarantee maximum exposure to the environment. To measure the content of drug and its degradation products, samples were dissolved using 15% deionized water in acetonitrile solution and analyzed using the HPLC. The crystal transitions were monitored by DSC and XRPD.

2.3 Results and Discussions:

2.3.1 Standard curve:

The linear concentration range for the FdCyd is 2-200 µg/mL at 215 nm and 20-200 µg/mL for THU at 195 nm. The correlation coefficient (r^2) values are greater than 0.998. The precision of intra-day and inter-day assay validation is less than 5%.

2.3.2 Separation:

The retention times of the FdCyd and THU are approximately 6.5 min and 16 min, respectively. A representative chromatogram of FdCyd in combination with THU is shown in Figure 2a. After 8 days at pH 2, three degradants were detected as shown in Figure 2b.

2.3.3 Degradation Mechanism of FdCyd:

The proposed degradation mechanism of FdCyd is the cleavage of the N-glycosidic bond to form the products shown in Figure 3. The spectrum of the one degradant is identical with the reference compound 5-fluorocytosine purchased from Sigma-Aldrich. Its molecular weight was confirmed by mass spectrometry as shown in Figure 4. Another degradant, 5-(hydroxymethyl)tetrahydrofuran-2,4-diol, was not detected by HPLC due to no chromophor in the molecule. The degradation mechanism of FdCyd does not change when THU is added to the solution.

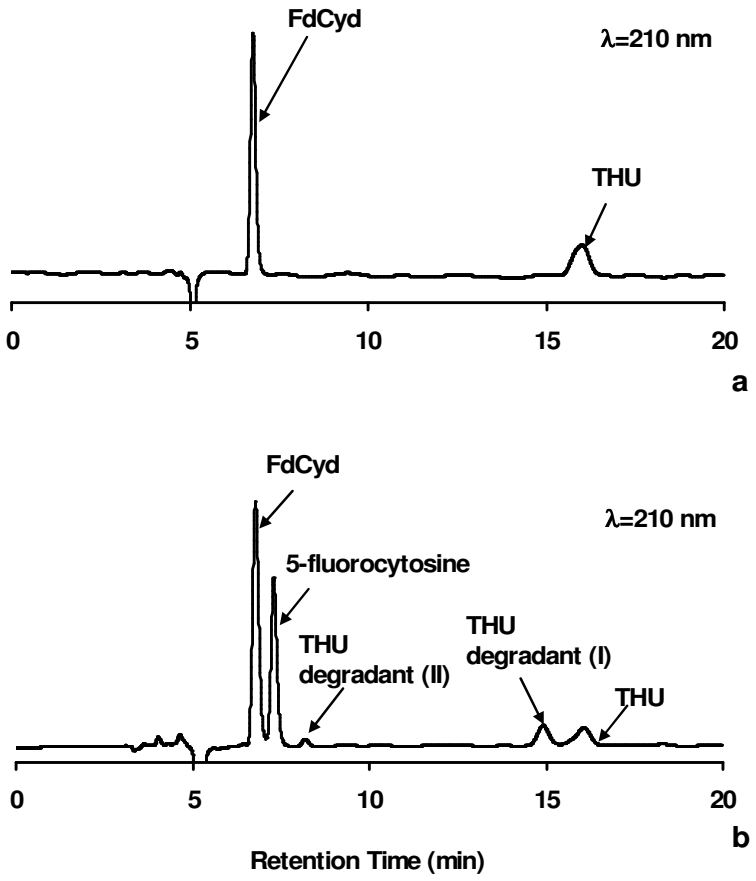

Figure 14: (a) Chromatograms of FdCyd and THU in combination at T=0,(b) chromatogram of FdCyd and THU and their degradants after 8 days at pH=2.

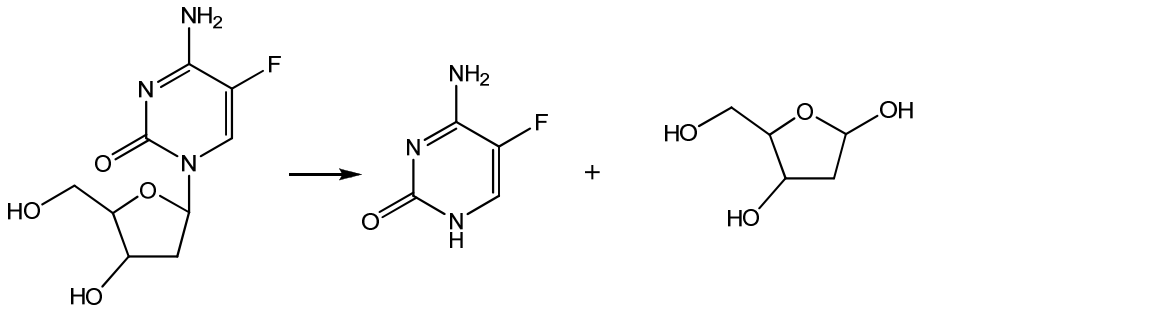

FdCyd **5-fluorocytosine** **5-(hydroxymethyl)tetrahydrofuran-2,4-diol**

Figure 15: Proposed degradation mechanism of FdCyd.

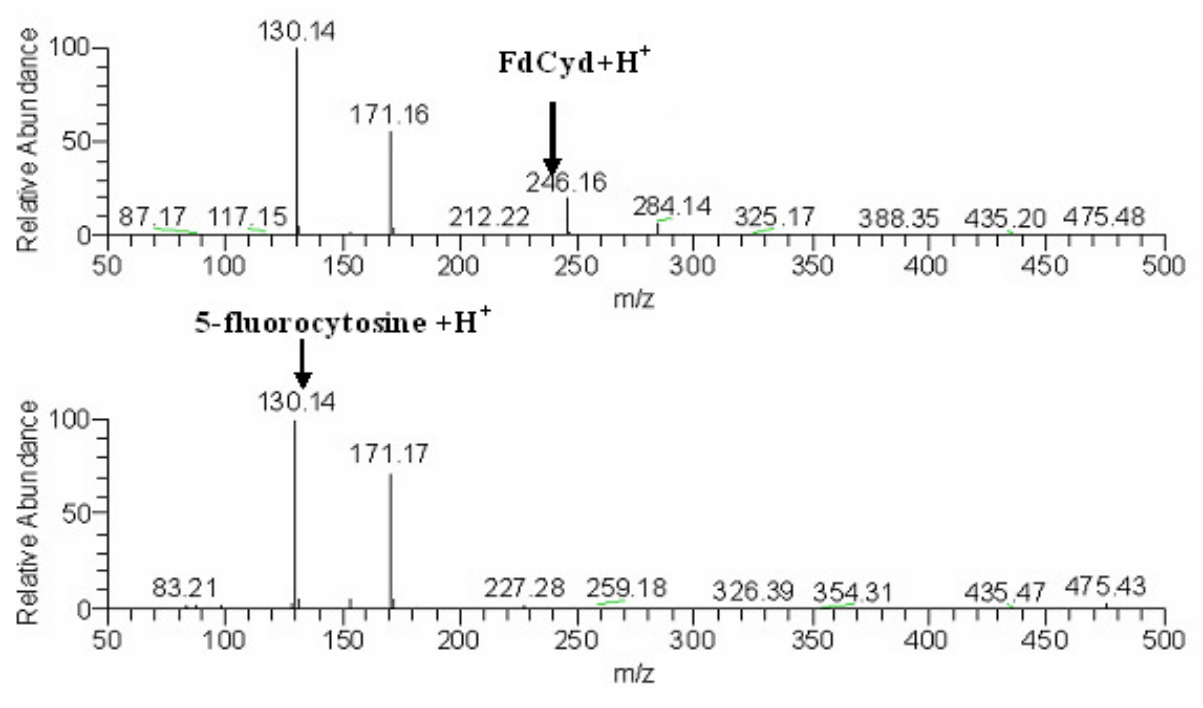

Figure 16: Mass spectra of FdCyd (top) and 5-fluorocytosine (bottom).

2.3.4 Degradation Mechanism of THU:

Tian *et al.* [12] conducted a thorough study of the interconversion, isomerization and hydrolysis of THU. THU decomposes by forming degradant (I) which is its ribopyranosyl isomer, degradant (II), and 5-(hydroxymethyl)tetrahydrofuran-2,3,4-triol which are hydrolysis products of slow N-glycosidic bond cleavage. Our results, shown in Figure 5 and Figure 6, are consistent with their results.

2.3.5 Degradation Kinetics of FdCyd:

The degradation of FdCyd in the presence of THU is nearly identical to that of pure FdCyd as shown in Figures 7a and 7b. In both cases, there are linear relationships between the logarithm of the remaining of FdCyd and the time described by

$$\log[D] = \log[D_0] - \left(\frac{k_{obs}}{2.303}\right) t$$

where $[D_0]$ and $[D]$ are the initial and time-dependent concentrations of drug, k_{obs} is the observed degradation rate constant, and t is time.

The k_{obs} data for FdCyd degradation with and without THU at various pH values are listed in Table 2 and illustrated graphically in Figure 8. It is clear that k_{obs} for FdCyd is dependent on the pH but not affected by THU. The stability of FdCyd improves with increase in pH and there is minimal degradation above pH 5.

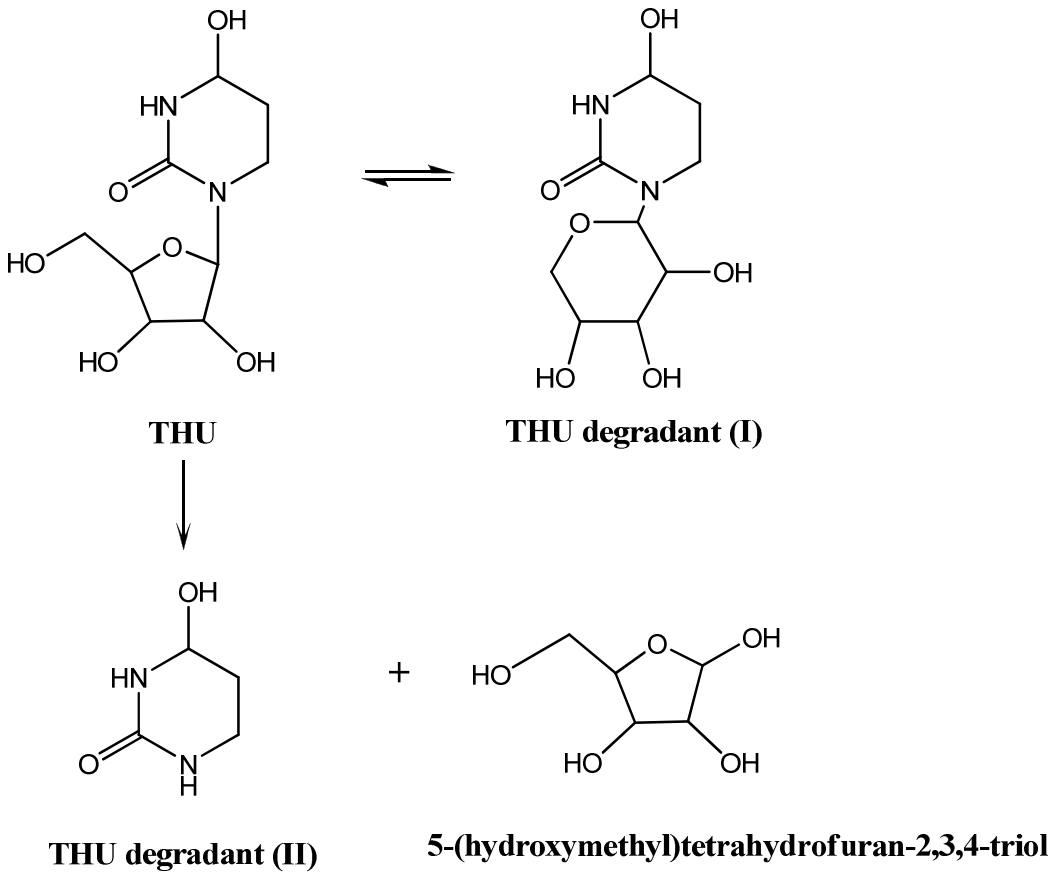

Figure 17: Degradation mechanism of THU.

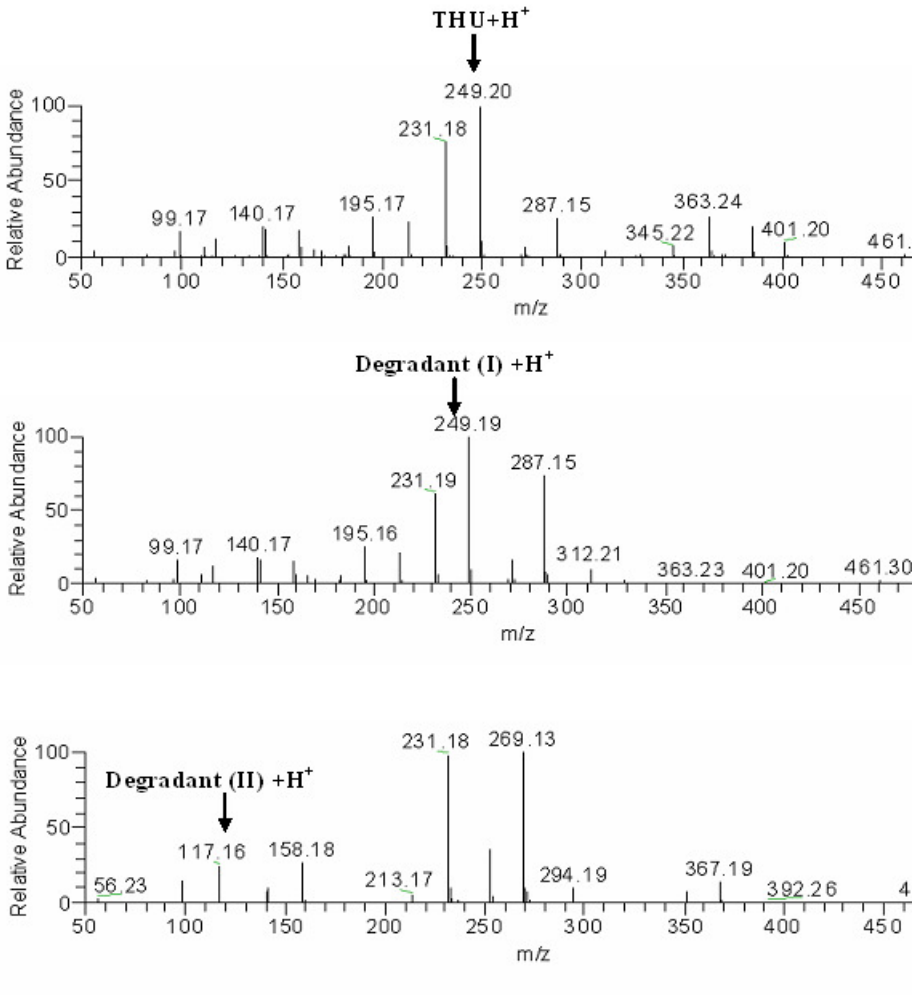

Figure 18: Mass spectra of THU (top) and degradant (I) (middle) and degradant (II) (bottom).

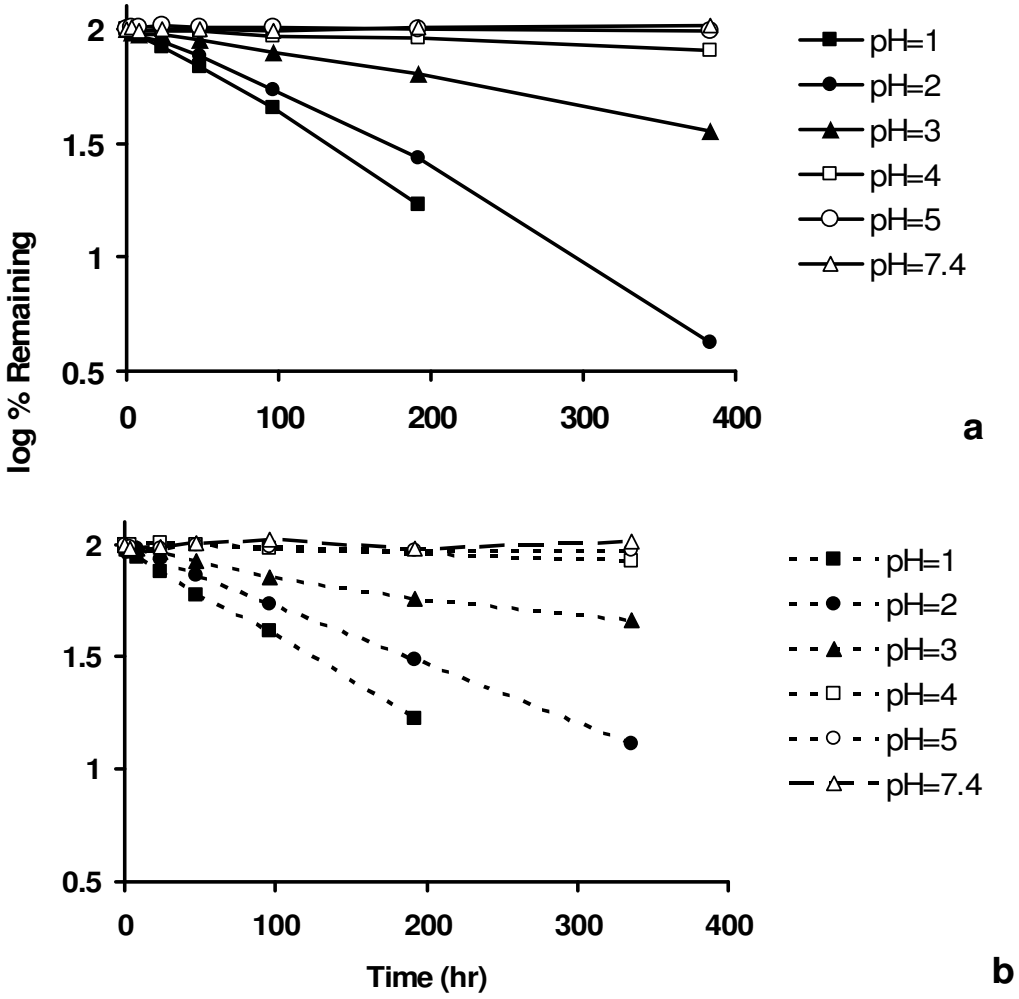

.

Figure 19: (a) Percentage remaining of FdCyd (in the absence of THU) vs. time; (b) percentage remaining of FdCyd (in the presence of THU) vs. time.

Table 8: Observed FdCyd degradation rate (hr^{-1}) in various solutions of different pH with and without THU.

pH	Alone	In combination with THU
1	0.00921	0.00898
2	0.00806	0.00599
3	0.00253	0.00230
4	0.000461	0.000461
5	0.000115	0.000138
7.4	0.000115	0.000092

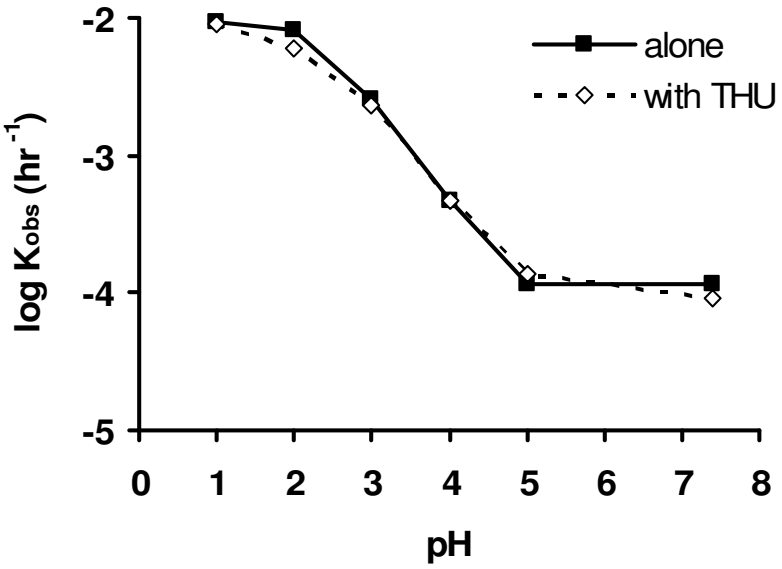

Figure 20: pH-log K_{obs} profile of FdCyd alone and in combination with THU at 37 ℃.

2.3.6 Degradation Kinetics of THU:

THU does not degrade by first-order kinetics. The flat minima in Figure 9a and 9b show that THU reaches equilibria with at least one of its degradation products. Like FdCyd, the degradation of THU is also acid-catalyzed and minimal above pH 5. The degradation profile of THU alone is not significantly different from that of THU in combination with FdCyd.

2.3.7 Light Effects on Solid State Stability:

The melting points of FdCyd and THU were determined to be approximately 205 °C and 150 °C. Upon 30 days of storage at ambient temperature in clear and amber vials, no significant degradation was detected by HPLC for solid FdCyd, THU or their 1:5 physical mixtures with and without grinding.

2.3.8 Temperature and Humidity effect on Solid State Stability:

The X-ray powder diffraction patterns of FdCyd and THU at T=0 are shown in Figure 21a and 21b, respectively. Changes in weight were not observed for any of the samples under 40 °C/ 75% RH after 1 month of storage. Results from XRPD, DSC and TGA show that no significant water absorption occurred during this time period. Degradants were not detected by HPLC, indicating FdCyd and THU are chemically compatible in solid state. Soft caking was noticed after two months for samples containing THU, which

suggests a slight interaction between the drug and moisture. However, hydrate formation was not observed using DSC and TGA.

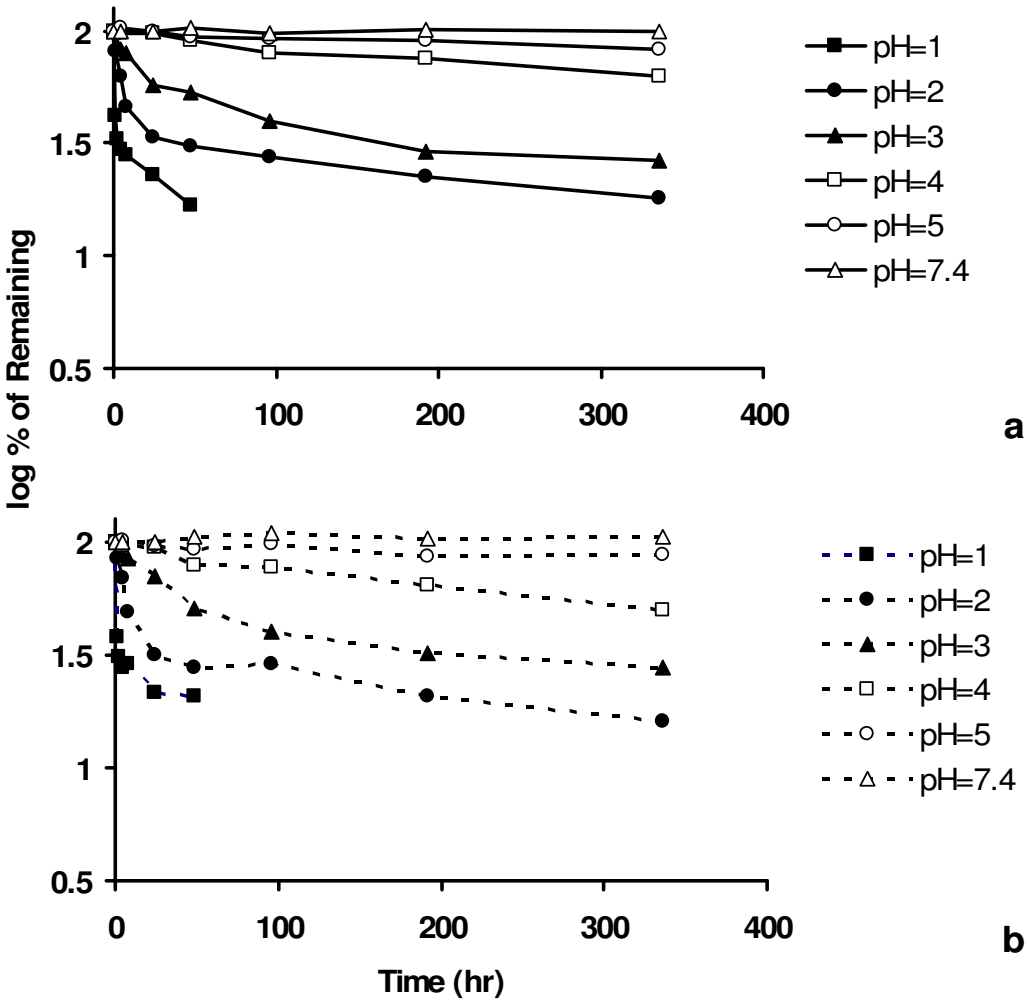

Figure 21: (a): Percentage remaining of THU (in the absence of FdCyd) vs. time; (b): percentage remaining of THU (in the presence of FdCyd) vs. time.

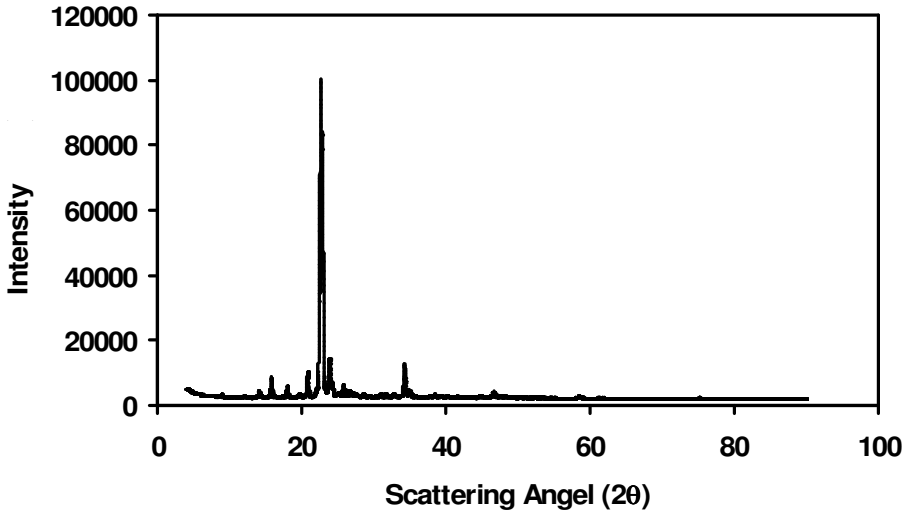

(a)

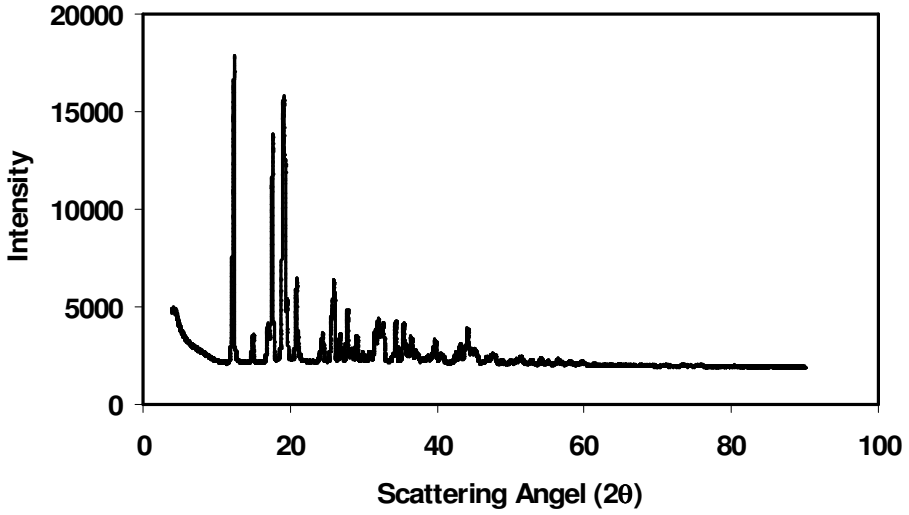

(b)

Figure 22: X-ray powder diffraction patterns for (a) FdCyd, (b) THU.

2.4 Conclusions:

An HPLC procedure that can separate FdCyd, THU and their degradants was developed. The degradation of FdCyd appears to be first order and an acid catalyzed reaction, whereas THU equilibrates with at least one of its degradants. Combining FdCyd and THU in the solution does not affect the degradation mechanism or kinetics of either compound. Light has no effect on the solid state stability at ambient temperature. Crystal transitions were not observed for samples stored under 40 °C/ 75% RH for a 1 month period.

CHAPTER 3: EFFECT OF POLARITY ON ACID-BASE DISSOCIATION IN IONIC MICELLE SYSTEMS

3.1 Background and Significance:

Micellar media are widely used in pharmaceutics, analytical chemistry, synthetic chemistry and many other fields [13,14]. One of the key properties of micelles is their ability to solubilize non-polar solutes which are insoluble in water. But the incorporation of an acid or a base by a micelle can result in a change of the dissociation constant of the solubilized species. Omar (1989) explained the shift of the dissociation constant in terms of differences between the properties of the bulk solvent and the micelle as well as the perturbation of the acid-base equilibrium by the electrostatic field of the charged interface.

Acid dissociation constants determine the extent of ionization of molecules in solution at any pH value. The chromatographic retention behavior and pharmaceutical properties like solubility, stability, toxicity, biological activity, etc., of a drug can be affected by its acid–base properties. Several techniques, including potentiometric titration and spectrophotometry, have been utilized to determine the acidity constants. [13,15-17].

3.1.1 Surfactants:

Surface active agents, or surfactants, possess both polar and non-polar moieties on the same molecule. As illustrated in Table 9, the polar region of a surfactant may carry a positive or negative charge, giving rise to cationic or anionic surfactant. Zwitterionic surfactants have polar regions that contain both anionic and cationic groups. The polar region of a non-ionic surfactant has no charge and can be composed of multiple polyoxyethylene groups, hydroxyl groups or a combination of these two. Owing to their unique structures, surfactants can aggregate and orient at interfaces as illustrated in Figure 23. At low concentrations, their tendency to be adsorbed onto the surfaces or interfaces significantly reduces the surface or interfacial free energy.

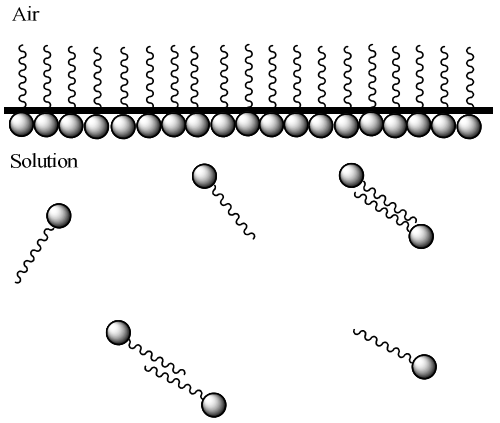

Figure 23: Schematic representation of surfactants aggregating at the air-solution interface. The polar region (○), and the non-polar hydrocarbon chain (〰) are schematically indicated to denote their relative locations but not their number, distribution.

Table 9: Examples of anionic, cationic, nonionic and zwitterionic surfactants.

ANIONIC:	
Sodium dodecyl sulphate (SDS)	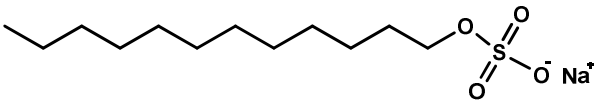
Sodium dodecylbenzene sulphonate	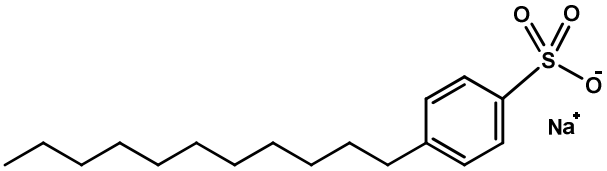
CATIONIC:	
Cetyltrimethylammonium bromide (CTAB)	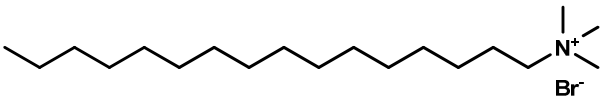
Cetyltrimethylammonium chloride (CTACl)	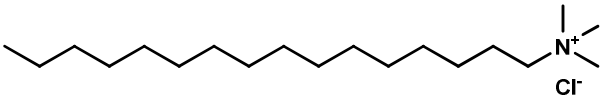
NON-IONIC:	
Polyoxyethylene lauryl ether (Brij 35)	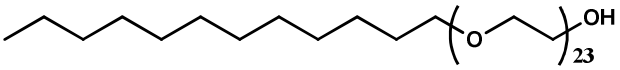
ZWITTERIONIC:	
Lecithins, e.g. phosphatidyl choline	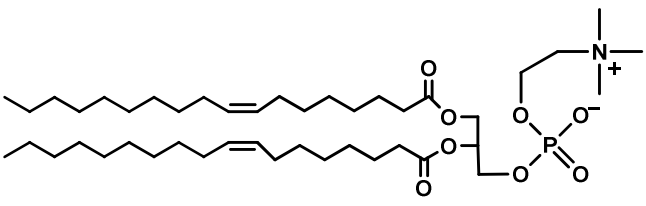

3.1.2 Micelle Formation:

In addition to the surface adsorption properties of surfactants, they can self-assemble in aqueous and non-aqueous solution by forming organized assemblies called micelles and reverse micelles, respectively. The concentration at which micelles begin to form is a characteristic of the particular surfactant and is called the critical micelle concentration (*cmc*). A schematic illustration of a typical micelle in water is given in Figure 24. The micelle has a nonpolar interior that is composed of the hydrocarbon moieties, and a surface that consists of the polar moieties. In dilute solution, surfactants exist as monomers and the solution has ideal physical and chemical properties. As the surfactant concentration increases, these properties deviate gradually from ideality and abrupt changes occur at the *cmc* when monomers aggregate into micelles. The driving force for micelle formation is to minimize the contact of the hydrophobic portion of the surfactant region with water (i.e., minimize surface energy).

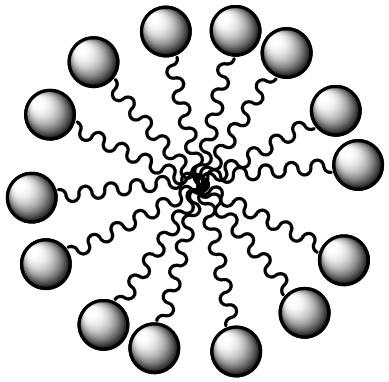

Figure 24: Schematic representation of micelle in aqueous solution.

3.1.3 Thermodynamic Models:

Two approaches, the pseudophase model and the equilibrium model, are commonly used to interpret micellar aggregation. In the pseudophase model, the micelle is considered as a separate phase [18,19]. Properties such as conductivity, surface tension and density show an abrupt change at the *cmc*. This behavior indicates a transition from a single phase to two phases. Thus, the *cmc* represents the saturation concentration of the monomer. The micelles would form above the *cmc* and constitute a separate pseudophase.

According to the other approach, the equilibrium model, micelles are dynamic structures, with monomers associating and dissociating between the micelles and the bulk solution [20-22]. The micelle can be treated as being formed by a stepwise aggregation in which an n-mer is in equilibrium with a single monomer and an (n-1)-mer, i.e.:

$$M_1 + M_{n-1} \leftrightarrow M_n \quad n = 2, 3\ldots. \qquad (1)$$

Alternatively, the micelle can be regarded as being formed by a single step aggregation from n monomers, i.e.:

$$nM_1 \leftrightarrow M_n \quad n = 2, 3\ldots. \qquad (2)$$

It is difficult to experimentally distinguish between these equilibrium models and the pseudophase model. However, the latter is more convenient for our purpose and will be used to interpret the studies of acid-base equilibria.

3.1.4 Factors that Affect Micellization:

The interplay among intermolecular effects, including electrostatic, hydrogen bonding, and van der Waals forces as well as steric effects, determines the organization of micellar systems [23,24]. In addition to the effect of hydrocarbon being squeezed out from water, there is a strong affinity between the polar group and water [25]. Whether the micellization occurs or not depends on the balance among all the interactions.

As stated above, micellization starts after the surfactant concentration reaches the *cmc*. The *cmc* can be controlled by changing the chemical structure of the surfactant as well as by varying solution conditions such as temperature, solvent polarity and pH [7]. Increasing temperature generally produces an increase in the *cmc* of an ionic surfactant and a slight decrease in the *cmc* of nonionic surfactants. A small amount of nonpolar impurity can lower the *cmc* by acting as a nucleus for micellization. Introducing a cosolvent to the system increases the solubility of monomer and thus increases the *cmc*. On the other hand, strong electrolytes salt-out surfactant molecules and produce a decrease in the *cmc*. For surfactants that contain weak electrolyte polar groups, the pH of the solution is the most significant factor that affects the *cmc*. A 50% increase of the *cmc* for cationic acyl carnitines over their neutral counterparts was reported [26].

3.1.5 Solubilization:

One particular significance of micelles in pharmaceutics is their ability to increase the solubility of poorly soluble substances in water [25,27]. Micelle structures are characterized by an anisotropic distribution of water. That is, the core of the micelle is composed almost entirely of the hydrocarbon moieties of the surfactant and is the most nonpolar region. The micelle surface that surrounds the core consists of hydrocarbon, polar moieties from the head of the surfactant and some penetrated water. The predominant location of a solubilized drug depends on its polarity and its interactions with the surfactant. Consequently, nonpolar molecules will most likely be incorporated in the core, while more polar compounds tend to locate closer to the surface.

The general equation for micellar solubilization is:

$$S_{tot} = S_w + \kappa(C_{surf} - CMC) = S_w + \kappa C_{mic} \approx S_w + \kappa C_{surf} \qquad (3)$$

where S_{tot} is the total solubility of the drug, S_w is the intrinsic water solubility, κ is the solubilization capacity of the surfactant for the drug, CMC is the critical micellar concentration, and C_{surf} and C_{mic} are the concentrations of total surfactant and micellar surfactant, respectively [7].

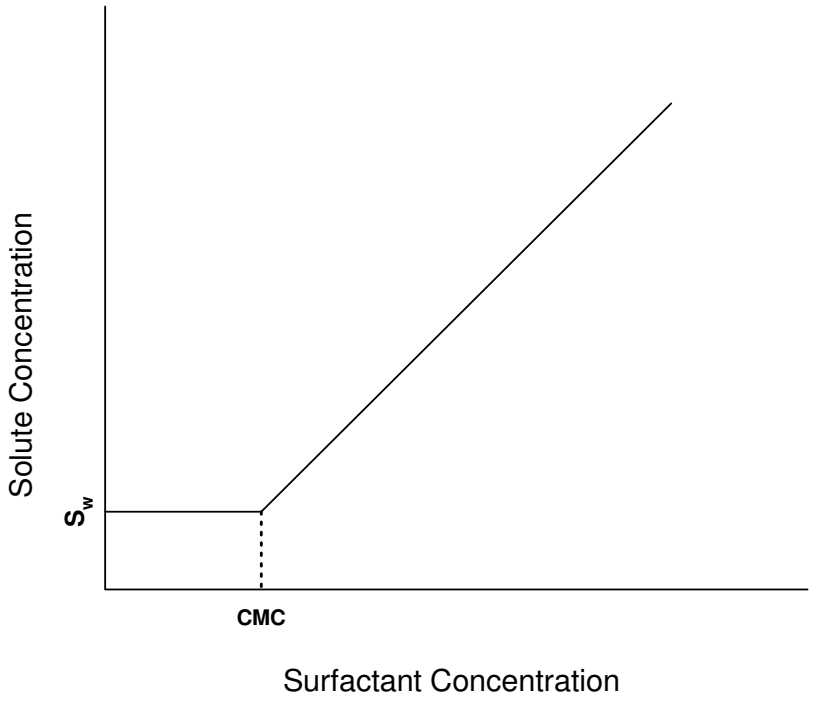

Figure 25: General solubilization curve for surfactants.

The micellar solubilization of a compound as a function of the concentration of surfactant is shown in Figure 25. The drug concentration is equal to the intrinsic solubility until the surfactant concentration reaches the *cmc*. Above the *cmc*, the solubility increases linearly with surfactant concentration. The surfactant solubilization capacity, κ, describes the amount of solute that can be solubilized by a given amount of surfactant. Another commonly used descriptor of solubilization is the micelle-water partition coefficient, P_M. It is defined as the ratio of the solute concentration in the micelle to that in the water. Thus, it can be related to κ as

$$P_M = \frac{\kappa (C_{surf} - CMC)}{S_w} = \frac{\kappa C_{mic}}{S_w} \approx \frac{\kappa C_{surf}}{S_w} \qquad (4)$$

Since P_M is restricted by the surfactant concentration, it will be convenient to normalize it with the surfactant concentration.

$$P_M^N = \frac{\kappa}{S_w} \tag{5}$$

The pH of a solution can alter the solubilization by affecting the degree of ionization of a weak electrolyte solute as well as a week electrolyte surfactant [7]. For a surfactant that is a strong electrolyte, the total solubility of a weak electrolyte solute is then given by:

$$S_{tot} = S_u + S_i + \kappa_u C_{mic} + \kappa_i C_{mic} \tag{6}$$

where S_u and S_i are solubilities of the unionized and ionized forms of the solute, κ_u and κ_i are the solubilization capacities for the unionized and ionized solute, respectively. When combined with Eq. (4) and Eq. (5), Eq. (6) can be expressed as

$$S_{tot} = S_u + S_i + S_u P_{Mu} + S_i P_{Mi} \tag{7}$$

which can be rearranged to

$$S_{tot} = S_u(1 + P_{Mu}) + S_i(1 + P_{Mi}) \tag{8}$$

Applying the Henderson-Hasselbalch equation to Eq. (8) gives a general relationship for the solubilization of a weak electrolyte by the synergism of surfactants and pH:

$$S_{tot} = S_u\left[(1 + P_{Mu}) + (1 + P_{Mi})10^{(pH - pK_a)}\right] \tag{9}$$

3.1.6 Effects of Micelles on Substrates:

As mentioned above, the ability to solubilize non-polar compounds is one of the major interests of micelles solution. Solubilization of a weak electrolyte in the micellar pseudophases can lead to pronounced perturbation of the kinetic and equilibrium properties of the solubilized species [28].

3.1.7 Kinetics in Micellar System:

Micelles can be utilized to accelerate organic reactions by concentrating the reactants within small volumes [29,30]. On the other hand, micelles can stabilize a substance by separating it form reactants in the solution [31,32]. Also, the reactivities of substrates may be changed due to their orientation in or on the micelle [33,34]. Thus chemical reactions can either be accelerated or retarded by micellization.

The above effects of micellization on reaction rates are the result of the microscopic properties of the micellar pseudophase compared with the bulk solvent. Measurements using lipoid pH probes adsorbed at the interface of micelles indicate that the effective polarities and dielectric constants of micelle are lower than those of water [35]. The interfacial potential of ionic and zwitterionic aqueous micelles can also contribute to the alteration in the reactivity of substrates [36]. Another possible mechanism is that micelle can solubilize a reactant that is not very soluble in the reaction medium. The reactant in micelle can thus serve as a reservoir and prolong the reactivity. Enhancement by 1000 times in the reaction rate has been reported, which makes micellar catalysis very attractive for potential applications.

3.1.8 Acid-base Equilibria in Micellar Systems:

The dissociation constant is often a determinant of the biological efficacy of a drug. The equilibrium between the dissociated and undissociated molecules of a weak acid (HA) in a solution is given as:

$$HA \leftrightarrow H^+ + A^- \tag{10}$$

The dissociation constant in water is

$$K_a^w = \frac{[H^+][A^-]}{[HA]} \tag{11}$$

Aqueous micelles have interfaces that are structurally similar to biological membranes, thus they are often used as models for studying the latter. The acid–base equilibrium for a weak acid located at an aqueous micellar phase can be represented as

$$HA_m \leftrightarrow H_m^+ + A_m^- \tag{12}$$

Since the hydrogen ion concentration at the micelle surface can not be measured, the apparent dissociation constant is defined as

$$K_a^{app} = \frac{[H_w^+][A_m^-]}{[HA_m]} \tag{13}$$

where subscripts '*m*' and '*w*' denote the micellar and bulk phases, respectively.

This pK_a shift by micelle phenomenon was first observed by Hartley [37]. His results show that the difference between the apparent pK_a in a micellar system, pK_a^{app}, and the value in water, pK_a^w, is related to the surface potential of the micelle, Ψ, by:

$$\Delta pK_a = pK_a^{app} - pK_a^w = -\frac{F\Psi}{2.303RT} \tag{14}$$

where F is the Faraday constant, R is the universal gas constant and T is the absolute temperature.

The surface potential of a micelle is dependent on its surface charge density σ^*, the thickness of the electrical double layer, D, as well as dielectric constant of the bulk water ε [38].

$$\Psi = \frac{\sigma^*}{\varepsilon D} \tag{15}$$

Moller et al. [39] found that increasing the ionic strength from 0.03 to 4.03 produced an increase of up to 1.66 units for the pK_a of several sulphophthaleins in the presence of CTACl. This is due to the fact that ionic strength of the aqueous phase and the type of ions present can affect the thickness of the electrical double layer and dielectric constant of the media.

Based on Eq. (13), non-ionic micelles (Ψ=0) are not expected to have an effect on the pK_a. However, Tong and Gleesmann [40] noticed that the pK_a values of weak electrolytes in non-ionic micelles Triton X-100 also shift slightly from their intrinsic values. This is due to the fact the dissociation of the solute may also be affected by the difference in the dielectric constants of its microenvironment and the bulk water. The pK_a shift induced by a charged interface is actually a combination of the medium effect and the electrostatic effect.

$$\Delta pK_a = f(\Psi, \varepsilon) \tag{16}$$

The shift in pK_a is also dependent on the partitioning of the species between the aqueous and micellar pseudophases. Taillardat-Bertschinger et al. [41] suggested that the apparent

ionization equilibrium depends not only on the surface potential and dielectric constant, but also on the partition of the solute into the micelle. Garrone et al. [42] studied the apparent ionization constants for a series of *m*- and *p*- substituted benzoic acids in the SDS micellar system. Their results show a good correlation between pK_a^{app} and π, where π is the substituent contribution to the octanol-water partition coefficient as defined by [43]. Therefore,

$$\Delta pK_a = f\left(\Psi, \varepsilon, \log P_m\right) \qquad (17)$$

3.1.9 Techniques:

Potentiometric titration is the most convenient method to determine the dissociation constant. The potential difference between the hydrogen and reference electrodes is used to measure the pH value. The pH will be measured with the successive addition of known increments of acidic or basic titrant. UV spectroscopy is a another technique for the determination of ionization constant [44]. Fluorescence has also been used for fluorescent compounds such as coumarin and naphthol [35,45] . However, these latter techniques can only be used under the condition that a significant spectral change occurs when the solute dissociates. Therefore they are not applicable for many drugs.

3.2 Model:

The surface potential of strong electrolyte micelle like SDS and CTAB, is independent of the pH of the solution. Likewise, the aggregation number (number of surfactant molecules per micelle) is constant. Therefore, both the electrostatic and dielectric effect of the micelle on the dissociation of the solute can be treated as constant. Thus, the pK_a shift is solely related to the extent of the partitioning of the solute into the micelle.

$$\Delta pK_a = f'\left(\log P_m\right) \qquad (18)$$

In order to quantify the magnitude of dissociation constant shift in micelles, it is necessary to utilize a model for the micelle. The proposed pseudophase-partitioning model was developed under the following assumptions and conditions.

- The micelle as a smooth, spherical particle.
- The net charge of the micelle is uniformly distributed over its surface.
- The change of the micelle properties (including the *cmc*) due to the presence of a solute can be neglected.
- The solute lies at or near the micelle surface and is available for titration.

Since the micelle is a dynamic system, it does not have a well defined aggregation number. However, the aggregation number is approximately constant over a broad concentration range (up to about 100 times the *cmc*), with the number of the micelles in the solution varying [46]. A mean aggregation number between 50 to 100 is generally used and there are only one or two drug molecules incorporated in each micelle [47,48]. Thus, it is safe to assume that the partition of a solute into a micelle does not affect micelle properties such as *cmc* and surface potential.

It is well known that the micellar partition coefficients of the hydrocarbons correlate with their octanol-water partition coefficients [7]. In our proposed model, the logarithm of the octanol-water partition coefficient of the substance, $\log P_{ow}$, will be used as the primary solute descriptor to quantitate the magnitude of the acid-base equilibrium shifts.

The driving force for the partition of a solute between water and the micelle is the same as that of partition between water and octanol. Linear relationships between the solute octanol-water partition coefficients and their partition coefficients into non-ionic micelles have been observed by Collete [49], Tomida [50] and Alvarez-Nunez [51]. These relationships have the general form of:

$$\log P_M^N = a + b \log P_{ow} \qquad (19)$$

where a and b are constants that depend on the surfactant.

Treiner and Mannebach [52] obtained similar regression equations using literature data for micellar partition coefficients in the anionic sodium lauryl sulfate-water system.

As illustrated in Figure 26, the partitioning of solute into the micelle can be related to the polarity of the solute. Combining Eq. (18) and Eq. (19), the pK_a shift in a fixed micellar system is dependent on $\log P_{ow}$.

$$\Delta pK_a = f''\left(\log P_{ow}\right) \qquad (20)$$

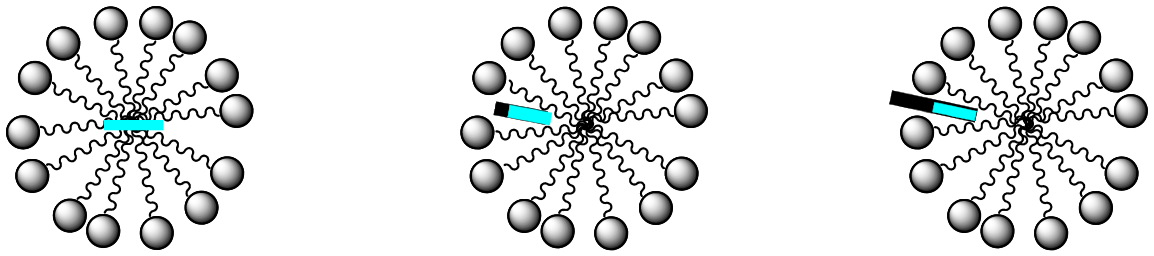

Figure 26: Partition of drug (■ represent polar portion, ■ represents nonpolar portion) in micelles.

3.3 Data Collection:

The reported pK_a^{app} of various acidic compounds in SDS and CTAB were collected from the literature. The effects of micelles on acid-base equilibria in aqueous solutions are provided in Table 10 and Table 11. These effects are given in terms of ΔpK_a, which represents the difference between the pK_a^{app} in micelle and pK_a^{w} in bulk aqueous solution. The dissociation constant values for some solutes have been determined in the presence of the same surfactant by several authors but under different temperature or different ionic concentration. The sign of ΔpK_a is usually the same but the magnitude of the value differs partially as the result of differences in the experimental conditions or experimental error.

Table 10: pK_a shift of acidic compounds in SDS micelle systems.

Compounds	ClogP	pK_a^w	ΔpK_a	References
1-Naphthalene acetic acid	2.59	4.10	1.04	[53]
2-Naphthoic acid	3.06	4.03	1.56	[53]
3-Acetylbenzoic acid	1.59	3.86	0.75	[42]
3-Bromobenzoic acid	2.85	3.85	1.22	[42]
3-Chlorobenzoic acid	2.70	3.87	1.03	[42]
3-Cyanobenzoic acid	1.55	3.67	0.60	[42]
3-Fluorobezoic acid	2.13	3.90	0.70	[42]
3-Hydroxybenzoic acid	1.56	4.13	0.59	[42]
3-Iodobenzoic acid	3.11	3.89	1.36	[42]
3-Methoxybenzoic acid	2.02	4.13	0.81	[42]
3-Methylbenzoic acid	2.38	4.33	0.96	[42]
3-Nitrobenzoic acid	1.84	3.51	0.68	[42]
4-Acetylbenzoic acid	1.59	3.73	0.76	[42]
4-Bromobenzoic acid	2.85	4.01	1.23	[42]
4-Chlorobenzoic acid	2.70	4.01	1.10	[42]
4-Fluorobezoic acid	2.13	4.19	0.64	[42]
4-Hydroxybenzoic acid	1.56	4.64	0.19	[42]
4-Iodobenzoic acid	3.11	3.96	1.40	[42]
4-Methoxybenzoic acid	2.02	4.54	0.74	[42]
4-Methylbenzoic acid	2.38	4.43	0.91	[42]
4-Nitrobenzoic acid	1.84	3.44	0.86	[42]
4-Nitrophenol	1.85	N/A	0.80	[54]
7-Hydroxycoumarin	1.62	7.8	0.50	[45]
Acetic acid	-0.19	4.7	0.00	[55]
Alizarine	3.28	7.2	1.50	[55]
Benzoic acid	1.89	4.26	0.54	[42]
Chloroacetic acid	-0.08	2.8	0.10	[55]
Dichloroacetic acid	0.98	1.5	0.10	[55]
Pindolol	1.67	9.50	0.47	[56]

Table 11: pK_a shift of acidic compounds in CTAB micelle systems.

Compounds	ClogP	pK_a^w	ΔpK_a	References
2,4-Dinitrophenol	1.82	4.06	-1.66	[57]
2,4-Dichlorophenol	2.97	8.17	-0.67	[58]
2-Amino-4-nitrophenol	1.18	7.00	-0.52	[57]
2-Bromo-4-nitrophenol	2.54	5.66	-1.01	[57]
2-Chloro-4-nitrophenol	2.34	5.42	-1.04	[57]
2-Nitro-4-bromophenol	2.82	6.38	-2.06	[57]
2-Nitro-4-carboethoxyphenol	2.54	5.42	-0.97	[57]
2-Nitro-4-carbomethoxyphenol	2.01	5.11	-1.10	[57]
2-Nitro-4-chlorophenol	2.67	6.49	-2.34	[57]
2-Nitro-4-iodophenol	3.08	6.24	-1.94	[57]
2-Nitro-4-methoxyphenol	1.93	7.41	-0.78	[57]
2-Nitro-4-methylphenol	2.54	7.53	-1.27	[57]
2-Nitro-4-tert-butylphenol	3.68	7.47	-1.30	[57]
2-Nitro-6-bromophenol	2.54	5.41	-1.95	[57]
2-Nitro-6-chlorophenol	2.34	5.42	-1.85	[57]
2-Nitrophenol	1.85	7.15	-1.24	[57]
3-Chlorophenol	2.48	8.93	-0.42	[58]
3-Methyl-4-nitrophenol	2.27	7.39	-0.56	[57]
3-Nitrophenol	1.85	8.18	-0.28	[57]
4-Chlorophenol	2.48	9.42	-0.58	[58]
4-Methoxyphenol	1.57	10.2	-0.10	[58]
4-Nitrophenol	1.85	7.15	-0.60	[57]
4-Nitrophenol	1.85	7.15	-0.95	[59]
4-Nitrophenol	1.85	7.15	-0.80	[60]
Acetic acid	-0.19	4.7	-0.10	[55]
Chloroacetic acid	-0.08	2.8	0.00	[55]
Dichloroacetic acid	0.98	1.5	0.00	[55]
Phenol	1.48	10.0	-0.30	[58]
p-tert-Butylphenol	3.30	10.13	-0.74	[61]

3.4 Results:

The calculated partition coefficients (ClogP^{TM}) of the compounds studied were obtained from Biobyte software and listed in Table 10 and 11. The ClogP values are plotted against the ΔpK_a values in the micellar system in Figure 27. The graph shows that anionic SDS micelles increase the pK_a of the solute, while cationic CTAB micelles decrease the pK_a.

The regression line of pK_a shift for acids in SDS is described by

$$\Delta pK_a = 0.552 \log P_{ow} - 0.369 \qquad (21)$$

n=30 r=0.836

Similar analysis was performed for acid in CTAB micelle and the relationship between the ClogP and pK_a shift is

$$\Delta pK_a = -0.487 \log P_{ow} + 0.115 \qquad (22)$$

n=29 r=0.239

It is clear that ΔpK_a of acids in sodium lauryl sulfate micelle is dependent on the octanol-water partition coefficient. In the case of acids in CTAB in Figure 27, the effect of polarity on the pK_a shift is obvious. However, due to the fact that all the data are reported by different workers where the experimental conditions were not quite the same, there is a lot of scatter in the data.

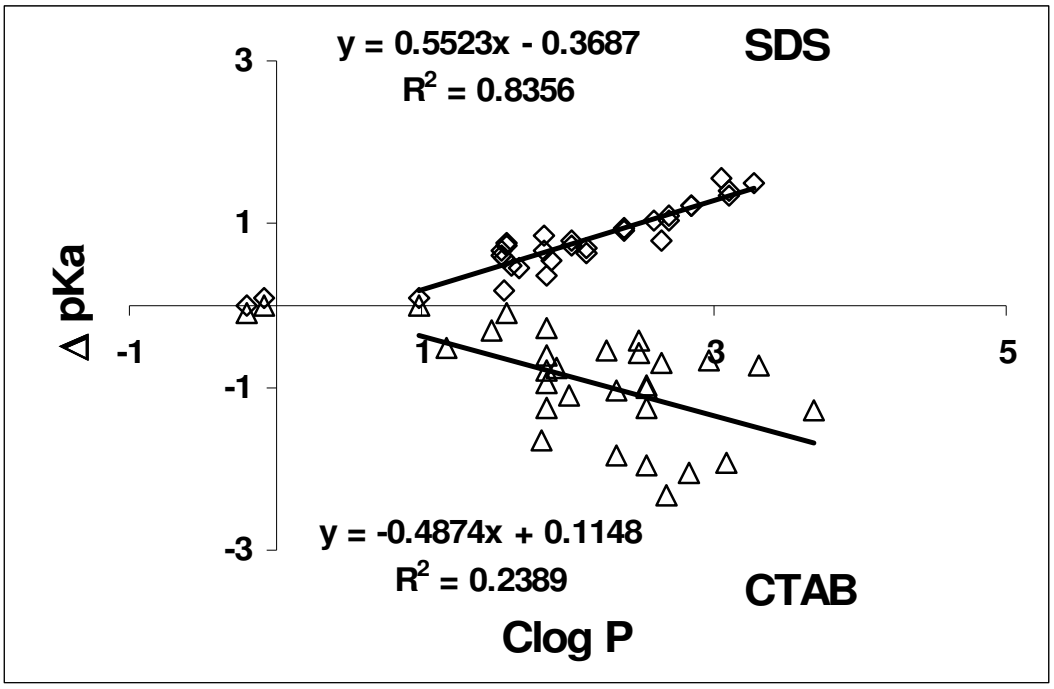

Figure 27: : pK_a shift of acids in anionic (SDS) and cationic (CTAB) micellar systems.

3.5 Conclusion:

The values of acid compounds pK_a shift in the anionic surfactant (SDS) and the cationic surfactant (CTAB) were compiled from the literature. Linear relationships exist between the polarity of the compounds and their pK_a shift in micelle system. The pKa values of acid tend to increase in the presence of anionic SDS micelles and decrease in the presence of cationic CTAB micelles.

REFERENCES:

1. Ge Y, Montano I, Rustici G, Freebern WJ, Haggerty CM, Cui W, Ponciano-Jackson D, Chandramouli GVR, Gardner ER, Figg WD, Abu-Asab M, Tsokos M, Jackson SH, Gardner K 2006. Selective leukemic-cell killing by a novel functional class of thalidomide analogs. Blood FIELD Full Journal Title:Blood 108(13):4126-4135.

2. Ng SSW, MacPherson GR, Guetschow M, Eger K, Figg WD 2004. Antitumor effects of thalidomide analogs in human prostate cancer xenografts implanted in immunodeficient mice. Clin Cancer Res FIELD Full Journal Title:Clinical Cancer Research 10(12, Pt. 1):4192-4197.

3. Ge Y, Byun JS, De Luca P, Gueron G, Yabe IM, Sadiq-Ali SG, Figg WD, Quintero J, Haggerty CM, Li QQ, De Siervi A, Gardner K 2008. Combinatorial Antileukemic Disruption of Oxidative Homeostasis and Mitochondrial Stability by the Redox Reactive Thalidomide 2-(2,4-Difluoro-phenyl)-4,5,6,7-tetrafluoro-1H-isoindole-1,3(2H)-dione (CPS49) and Flavopiridol. Mol Pharmacol 74(3):872-883.

4. Ng SSW, Gutschow M, Weiss M, Hauschildt S, Teubert U, Hecker TK, Luzzio FA, Kruger EA, Eger K, Figg WD 2003. Antiangiogenic activity of N-substituted and tetrafluorinated thalidomide analogues. Cancer Res 63(12):3189-3194.

5. Kumar S, Raje N, Hideshima T, Ishitsuka K, Roccaro A, Shiraishi N, Hamasaki M, Yasui H, Munshi NC, Richardson P, Figg WD, Anderson KC 2005. Antimyeloma activity of two novel N-substituted and tetraflourinated thalidomide analogs. Leukemia 19(7):1253-1261.

6. Warfel NA, Lepper ER, Zhang C, Figg WD, Dennis PA 2006. Importance of the Stress Kinase p38alpha in Mediating the Direct Cytotoxic Effects of the Thalidomide Analogue, CPS49, in Cancer Cells and Endothelial Cells. Clin Cancer Res FIELD Full Journal Title:Clinical Cancer Research 12(11, Pt. 1):3502-3509.

7. Yalkowsky SH. 1999. Solubility and solubilization in aqueous media. ed., New York: Oxford University.

8. Beumer JH, Eiseman JL, Parise RA, Joseph E, Holleran JL, Covey JM, Egorin MJ 2006. Pharmacokinetics, Metabolism, and Oral Bioavailability of the DNA

Methyltransferase Inhibitor 5-Fluoro-2'-Deoxycytidine in Mice. Clin Cancer Res 12(24):7483-7491.

9. Beumer J, Parise R, Newman E, Doroshow J, Synold T, Lenz H-J, Egorin M 2008. Concentrations of the DNA methyltransferase inhibitor 5-fluoro-2′ -deoxycytidine (FdCyd) and its cytotoxic metabolites in plasma of patients treated with FdCyd and tetrahydrouridine (THU). Cancer Chemotherapy and Pharmacology 62(2):363-368.

10. Stoller RG, Myers CE, Chabner BA 1978. Analysis of cytidine deaminase and tetrahydrouridine interaction by use of ligand techniques. Biochemical Pharmacology 27(1):53-59.

11. Boothman DA, Briggle TV, Greer S 1987. Tumor-selective Metabolism of 5-Fluoro-2'-deoxycytidine Coadministered with Tetrahydrouridine Compared to 5-Fluorouracil in Mice Bearing Lewis Lung Carcinoma. Cancer Res 47(9):2354-2362.

12. Tian-Xiang Xiang RNPBBDA 2003. Epimer interconversion, isomerization, and hydrolysis of tetrahydrouridine: Implications for cytidine deaminase inhibition. Journal of Pharmaceutical Sciences 92(10):2027-2039.

13. Underwood AL 1977. Acid--base titrations in aqueous micellar systems. Analytica Chimica Acta 93:267-273.

14. Burguera JL, Burguera M 2004. Analytical applications of organized assemblies for on-line spectrometric determinations: present and future. Talanta 64(5):1099-1108.

15. Kubista M, Sjoeback R, Albinsson B 1993. Determination of equilibrium constants by chemometric analysis of spectroscopic data. Anal Chem 65(8):994-998.

16. Kara D, Alkan M 2000. Determination of acidity constants of acid-base indicators by second-derivative spectrophotometry. Spectrochimica Acta Part A: Molecular and Biomolecular Spectroscopy 56(14):2753-2761.

17. Jaiswal PV, Ijeri VS, Srivastava AK 2005. Effect of surfactants on the dissociation constants of ascorbic and maleic acids. Colloids and Surfaces B: Biointerfaces 46(1):45-51.

18. Bunton CA, Nome F, Quina FH, Romsted LS 1991. Ion binding and reactivity at charged aqueous interfaces. Acc Chem Res 24(12):357-364.

19. Harwell JH, Hoskins JC, Schechter RS, Wade WH 1985. Pseudophase separation model for surfactant adsorption: isomerically pure surfactants. Langmuir 1(2):251-262.

20. Aniansson EAG, Wall SN 1974. Kinetics of step-wise micelle association. J Phys Chem 78(10):1024-1030.

21. Aniansson EAG, Wall SN 1975. Kinetics of step-wise micelle association. Correction and improvement. J Phys Chem 79(8):857-858.

22. Wall SN, Aniansson GEA 1980. Numerical calculations on the kinetics of stepwise micelle association. J Phys Chem 84(7):727-736.

23. Tanford C. 1980. The hydrophobic effect: Formation of micelles and biological membranes. ed., New York: Wiley.

24. Wennerstrom H, Lindman B 1979. Micelles. Physical chemistry of surfactant association. Physics Reports 52(1):1-86.

25. Carlota Oliveira Rangel-Yagui1 APJ, Leoberto Costa Tavares 2005. Micellar solubilization of drugs.

26. Yalkowsky SH, Zografi G 1970. Some micellar properties of long-chain acylcarnitines. Journal of Colloid and Interface Science 34(4):525-533.

27. Narang AS, Delmarre D, Gao D 2007. Stable drug encapsulation in micelles and microemulsions. International Journal of Pharmaceutics 345(1-2):9-25.

28. Park S-H, Choi H-K 2006. The effects of surfactants on the dissolution profiles of poorly water-soluble acidic drugs. International Journal of Pharmaceutics 321(1-2):35-41.

29. Duynstee EFJ, Grunwald E 1959. Organic Reactions Occurring in or on Micelles. I. Reaction Rate Studies of the Alkaline Fading of Triphenylmethane Dyes and

Sulfonphthalein Indicators in the Presence of Detergent Salts. J Am Chem Soc 81(17):4540-4542.

30. Bacaloglu R, Bunton CA, Ortega F 1989a. Micellar enhancements of rates of SN2 reactions of halide ions: the effect of head group size. J Phys Chem 93(4):1497-1502.

31. Albrizzio J, Archila J, Rodulfo T, Cordes EH 1972. Secondary valence force catalysis. XIII. Kinetics of the alkaline fading of crystal violet in the presence of cationic surfactants. J Org Chem 37(6):871-874.

32. Bunton CA, Carrasco N, Huang SK, Paik CH, Romsted LS 1978. Reagent distribution and micellar catalysis of carbocation reactions. J Am Chem Soc 100(17):5420-5425.

33. TaScioglu S 1996. Micellar solutions as reaction media. Tetrahedron 52(34):11113-11152.

34. Bacaloglu R, Bunton CA, Cerichelli G, Ortega F 1989b. NMR study of the location of bromide ion and methyl naphthalene-2-sulfonate in cationic micelles: relation to reactivity. J Phys Chem 93(4):1490-1497.

35. Fernandez MS, Fromherz P 1977. Lipoid pH indicators as probes of electrical potential and polarity in micelles. J Phys Chem 81(18):1755-1761.

36. Broxton TJ, Marcou V 1991. Micellar catalysis of organic reactions. 29. SNAr reactions with neutral nucleophiles. J Org Chem 56(3):1041-1044.

37. Hartley GS 1934. The effect of long-chain salts on indicators: the valence-type of indicators and the protein error. Trans Faraday Soc:444 - 450.

38. Tokiwa F 1972. Electrostatic and electrokinetic potentials of surfactant micelles in aqueous solutions. Advances in Colloid and Interface Science 3(4):389-424.

39. Moller JV, Kragh-Hansen U 1975. Indicator dyes as probes of electrostatic potential changes on macromolecular surfaces. Biochemistry 14(11):2317-2323.

40. Tong LKJ, Glesmann MC 1957. The Mechanism of Dye Formation in Color Photography. V. The Effect of a Non-ionic Surfactant on the Ionization of Couplers. J Am Chem Soc 79(16):4305-4310.

41. Taillardat-Bertschinger A, Perry CS, Galland A, Prankerd RJ, Chairman WN 2003. Partitioning of halofantrine hydrochloride between water, micellar solutions, and soybean oil: Effects on its apparent ionization constant. Journal of Pharmaceutical Sciences 92(11):2217-2228.

42. Garrone A, Marengo E, Fornatto E, Gasco A 1992. A Study on pk_a^{app} and Partition-Coefficient of Substituted Benzoic-Acids in SDS Anionic Micellar System. Quantitative Structure-Activity Relationships 11(2):171-175.

43. Fujita T, Iwasa J, Hansch C 1964. A New Substituent Constant, π, Derived from Partition Coefficients. J Am Chem Soc 86(23):5175-5180.

44. Albert AaEPS. 1984. The determination of ionization constants : a laboratory manual. third ed., London ; New York Chapman and Hall.

45. Montal M, Gitler C 1973. Surface potential and energy-coupling in bioenergy-conserving membrane systems. Journal of Bioenergetics and Biomembranes 4(3):363-382.

46. Hiemenz PC, Rajagopalan, R. 1997. Principles of colloid and surface chemistry. 3ed ed., New York: Marcel Decker.

47. L. Sepulveda RS 1978. Micellar solubilization of apolar molecules. Die Makromolekulare Chemie 179(3):765-771.

48. Bales BL, Messina L, Vidal A, Peric M, Nascimento OR 1998. Precision Relative Aggregation Number Determinations of SDS Micelles Using a Spin Probe. A Model of Micelle Surface Hydration. J Phys Chem B 102(50):10347-10358.

49. Collete JHaK, L. 1975. Interaction of substituted benzoic acid derivatives with polysorbate 20 micelles. J Pharm Sci 64:1253–1255.

50. Tomida H, Yotsuyanagi, T. and Ikeda, K. 1978. Solubilization of benzoic acid derivatives by polyoxyethylene lauryl ether. Chem Pharm Bull 26:2821–2831.

51. Alvarez-Nunez FA, Yalkowsky SH 2000. Relationship between Polysorbate 80 solubilization descriptors and octanol-water partition coefficients of drugs. International Journal of Pharmaceutics 200(2):217-222.

52. Treiner C, Mannebach MH 1987. Correlation analysis of solubilization data in aqueous cationic and anionic micellar solutions: Case of the halocarbons. Journal of Colloid and Interface Science 118(1):243-251.

53. Underwood AL 1982. Dissociation of acids in aqueous micellar systems. Analytica Chimica Acta 140(1):89-97.

54. Herries DG, Bishop W, Richards FM 1964. The Partitioning of Solutes between Micellar and Aqueous Phases: Measurement by Gel Filtration and Effect on the Kinetics of Some Bimolecular Reactions. J Phys Chem 68(7):1842-1852.

55. Berthod A, Saliba C 1985. Mesures de pH en milieux micellaires
Analusis 13(10):437-442.

56. de Castro B, Domingues V, Gameiro P, Lima JLFC, Oliveira A, Reis S 1999. Acid-base properties and solubility of pindolol, diazepam and chlordiazepoxide in SDS micelles. International Journal of Pharmaceutics 187(1):67-75.

57. Seguchi K 1979. Effects of surfactats on the visible spectra and acidity of substitued nitrophenols. 56029n 28:20-25.

58. Lapinte C, Viout P 1974. Etude des effets des micelles cationiques sur l'etat initial et l'etat de transition de reactions nucleophiles anioniques. Tetrahedron Letters 15(38):3439-3442.

59. Meyer G, Viout P, Tchoubar B 1974. Accroissement de la fonction d'acidite H_ par effet micellaire. Tetrahedron Letters 15(29):2487-2490.

60. Minch MJ, Giaccio M, Wolff R 1975. Effect of cationic micelles on the acidity of carbon acids and phenols. Electronic and proton nuclear magnetic resonance spectral studies of nitro carbanions in micelles. J Am Chem Soc 97(13):3766-3772.

61. Bunton CA, Romsted LS, Sepulveda L 1980. A quantitative treatment of micellar effects upon deprotonation equilibriums. J Phys Chem 84(20):2611-2618.